NASA TECHNICAL NOTE

NASA TN D-7860

NASA TN D-7860

ANALYSIS OF VARIOUS DESCENT TRAJECTORIES FOR A HYPERSONIC-CRUISE, COLD-WALL RESEARCH AIRPLANE

Pierce L. Lawing

Langley Research Center
Hampton, Va. 23665

NATIONAL AERONAUTICS AND SPACE ADMINISTRATION • WASHINGTON, D. C. • JUNE 1975

1. Report No.	2. Government Accession No.	3. Recipient's Catalog No.
NASA TN D-7860		

4. Title and Subtitle	5. Report Date
ANALYSIS OF VARIOUS DESCENT TRAJECTORIES FOR A HYPERSONIC-CRUISE, COLD-WALL RESEARCH AIRPLANE	June 1975
	6. Performing Organization Code

7. Author(s)	8. Performing Organization Report No.
Pierce L. Lawing	L-9778
	10. Work Unit No. 505-11-31-02

9. Performing Organization Name and Address	11. Contract or Grant No.
NASA Langley Research Center Hampton, Va. 23665	

12. Sponsoring Agency Name and Address	13. Type of Report and Period Covered
National Aeronautics and Space Administration Washington, D.C. 20546	Technical Note
	14. Sponsoring Agency Code

15. Supplementary Notes

16. Abstract

The envelope of probable descent operating conditions for a hypersonic air-breathing research airplane has been examined. Descents selected included descents at cruise angle of attack, descents at high dynamic pressure, descents at high lift coefficient, descents with turns, and descents with drag brakes. These descents were parametrically exercised and compared from the standpoint of cold-wall (367 K) aircraft heat load. The descent parameters compared were total heat load, peak heating rate, time to landing, time to end of heat pulse, and range. Trends in total heat load as a function of cruise Mach number, cruise dynamic pressure, angle-of-attack limitation, pull-up g-load, heading angle, and drag-brake size are presented.

17. Key Words (Suggested by Author(s))	18. Distribution Statement
Descent trajectories Aircraft heat load Drag brakes	Unclassified – Unlimited New Subject Category 02

19. Security Classif. (of this report)	20. Security Classif. (of this page)	21. No. of Pages	22. Price*
Unclassified	Unclassified	60	$4.25

*For sale by the National Technical Information Service, Springfield, Virginia 22151

ANALYSIS OF VARIOUS DESCENT TRAJECTORIES FOR A HYPERSONIC-CRUISE, COLD-WALL RESEARCH AIRPLANE

Pierce L. Lawing
Langley Research Center

SUMMARY

The envelope of probable descent operating conditions for a hypersonic air-breathing research airplane has been examined. Descents selected included descents at cruise angle of attack, descents at high dynamic pressure, descents at high lift coefficient, descents with turns, and descents with drag brakes. These descents were parametrically exercised and compared from the standpoint of cold-wall (367 K) aircraft heat load. The descent parameters compared were total heat load, peak heating rate, time to landing, time to end of heat pulse, and range. Trends in total heat load as a function of cruise Mach number, cruise dynamic pressure, angle-of-attack limitation, pull-up g-load, heading angle, and drag-brake size are presented.

INTRODUCTION

Air-breathing, hydrogen-fueled aircraft offer a range of economic, ecological, and military advantages. These advantages are well documented (ref. 1) and have prompted proposals for a hypersonic research airplane program to provide a focus for hypersonic technology. Such a hypersonic program would provide performance information on integrated engine-airframe configurations and on the aircraft and associated thermal protection systems in the hypersonic flight regime. This knowledge is an essential prelude to the efficient design of air-breathing hypersonic aircraft.

To realize a near-term economical research vehicle that will effectively demonstrate and establish the use of advanced concepts in hypersonic technology, a small research airplane is envisioned (ref. 1) which employs liquid-hydrogen-fueled engines and conventionally fabricated aluminum structures with a suitable thermal protection system. A sizable portion of the flight time, range, and heat load during the mission of such a hypersonic research aircraft will occur during the descent phase and will affect the vehicle design.

To determine the effects of the descent phase on both mission planning and aircraft design, an analytical study was undertaken in which a variety of descent types were investigated with the aid of high-speed computers. From the results of this study, various types

of descent were selected for parametric analysis. The selection criteria were no engine power available, no negative lift conditions, equilibrium flight except for some transition maneuvers, coverage of the flight operations envelope available to the aircraft, low g-loads and a simple, nonoscillatory flight path.

The purpose of this paper is to present the results of these parametric analyses which show preliminary trends in total heat load, peak heating rate, time to landing, time to end of heat pulse, and downrange distance. Variables include cruise Mach number, cruise dynamic pressure, lateral range, g-loads, vehicle angle-of-attack capability, heading angle, and drag-brake size. Although the results reflect the philosophy inherent in a research aircraft program, they should be useful in the preliminary design of a hypersonic aircraft, particularly in the planning of abort descent models.

SYMBOLS

C_D	drag coefficient
C_L	lift coefficient
g	acceleration due to gravity
h	altitude
L/D	lift-drag ratio
M	Mach number
Q	total heat load
$\dot{Q}$	aircraft heating rate
q	dynamic pressure
S	drag-brake surface area
S_R	aircraft reference area (99.88 m^2)
T_w	wall temperature
t	time

V	velocity
α	angle of attack
ϕ	roll angle
ψ	heading angle

Subscripts:

c	cruise
2g	reference 2g pull-up maneuver
r	reference cruise dynamic pressure, 23.94 kPa (500 lb/ft^2)
$\psi=0^o$	zero heading angle

ANALYTICAL PROCEDURE

The configuration shown in figures 1 and 2 is the research aircraft used throughout this study (ref. 1). Aerodynamic and heating information were obtained over a range of Mach number, dynamic pressure and angle of attack by the use of the Hypersonic Arbitrary-Body Aerodynamic Computer Program (refs. 2 and 3). This computer code was modified by means of the Spalding-Chi method (ref. 4) to calculate heating with all-turbulent flow and cold-wall conditions $\left(T_w = 367\ K\right)$ assumed. The calculated aerodynamic and heating data used in this study are given in appendix A.

An existing descent trajectory code was modified to accept total aircraft heating rate as a function of Mach number, dynamic pressure, and angle of attack. A triple-interpolation scheme was utilized to determine the heating rate for each trajectory point. The heating rate, as well as its integrated value over the time of the descent, was listed for the trajectory. The descent code numerically solves the equations of motion for three degrees of freedom (ref. 5) with constant gravity and a nonrotating spherical Earth assumed.

PRESENTATION OF RESULTS

A value of 23.94 kPa (500 lb/ft^2) was chosen as a reasonable dynamic pressure for aircraft cruise. This cruise condition is the initial point of the descent trajectory. Since

there are an infinite variety of descent paths, it is reasonable to choose for investigation those which compose an envelope of possible operating conditions and a few special cases of interest in between. The two cases which provide the boundaries of the envelope are a descent at the highest dynamic pressure for which the vehicle is designed and a descent at the highest angle-of-attack capability of the vehicle. One of the midenvelope paths of special interest is the path the aircraft would follow during descent from the cruise altitude at the cruise angle of attack. This path, called the nominal descent, requires no transition maneuver and it is the first of the descent types presented.

Nominal Descent

To provide a reference point, a descent family was generated by allowing the aircraft to descend at a constant angle of attack equal to that at cruise. The descent angle of attack was that which provided equilibrium, or cruise, flight at a dynamic pressure of 23.94 kPa (500 lb/ft^2) over a range of Mach number. This dynamic pressure q_r and a Mach number of 8 will be referred to as the reference cruise condition. Figure 3 shows the relationship between L/D, α, and q/q_r.

A sample of the nominal descent from the reference cruise condition is presented in figure 4, where altitude, angle of attack, velocity, and heating rate are plotted as a function of time. Figure 5 shows total heat load integrated over the time of the descent as a function of cruise Mach number at several ratios of cruise dynamic pressure to the reference value q_r. The insert in figure 5 shows the variation in total heat load with cruise dynamic pressure for several cruise Mach numbers. The figure indicates that the total descent heat load is essentially insensitive ($Q/Q_r \approx 1$) to cruise dynamic pressure for $q/q_r > 0.8$.

High-Dynamic-Pressure Descent

Figure 6 presents a schematic of a high-dynamic-pressure descent as an altitude-Mach number plot. The aircraft starts at the reference cruise condition and maneuvers (descends) to a high-dynamic-pressure path for the major portion of the descent. The transition between the cruise and the descent dynamic pressure was accomplished by flying a zero-lift trajectory at the end of cruise. A 1° angle of attack for this aircraft provides approximately zero lift (fig. 3). The aircraft then falls, which results in a decrease in altitude, a more negative flight-path angle, and an increase in dynamic pressure. A pull-up maneuver is necessary to prevent the aircraft from undershooting the desired high-dynamic-pressure path.

To arrive at the desired dynamic-pressure path at the proper flight-path angle, a value of q between the cruise value and the desired descent-path value is chosen and the angle of attack is increased to the value necessary to increase the lift force to twice the aircraft weight. This maneuver is called the $2g$ pull-up and is maintained until the

desired high-dynamic-pressure path is reached. The flight-path angle is then examined to determine whether it is a value that will allow the aircraft to remain on the high-dynamic-pressure path; typically, the value is between 0° and -4.0°. If this condition is not met, the 2g pull-up initiation point is then iterated until the proper flight-path angle is achieved and the vehicle descends on the high-dynamic-pressure path, where the angle of attack is changed to the equilibrium angle of attack for this flight condition. If the aircraft deviates from the selected path, the angle of attack is returned to either the 2g value or zero as needed to correct the deviation.

An example of the high-dynamic-pressure descent is presented in figure 7, where velocity, altitude, heating rate, and angle of attack are presented as a function of time. This is a descent at a dynamic pressure of 71.82 kPa (1500 lb/ft^2) in which the constant high-dynamic-pressure portion begins at 54 sec. (Deviations from 71.82 kPa (1500 lb/ft^2) are within ±5 percent.) Figure 8 presents total heat load integrated over the descent time interval as a function of cruise Mach number for this type of descent.

High-Lift-Coefficient Descents

Previous studies have indicated that low heat loads result when the aircraft descends at a high lift coefficient (ref. 6). This condition requires the aircraft to turn a large amount of flow, compared with cruise flight at lower lift coefficients, and the aircraft creates a large wake, which dissipates a higher percentage of kinetic energy without increasing the airframe heat load. The lift coefficient available to a cruising aircraft is limited by the angle of attack its aerodynamic controls permit and by the structural loads imposed by the high lift force. Since the aircraft can presumably be designed to operate at any angle of attack for which the designer is willing to provide controls, there is no simple choice for maximum angle of attack; therefore, it is necessary to consider descents over a range of angle of attack in order to provide design trade-off information.

Descents with pull-up at constant angle of attack.- To investigate descents over a range of angle of attack, a pull-up at constant angle of attack was performed $\left(\alpha_{\text{pull-up}} < \alpha_{\text{descent}}\right)$ until the altitude for zero flight-path angle for the given pull-up maneuver was reached; this altitude was then examined to determine how well it approximated that required for equilibrium flight at the desired descent angle of attack. Next, the pull-up angle of attack was iterated to provide the altitude and velocity at zero flight-path angle that would sustain equilibrium flight at the desired descent angle of attack. This phase of the trajectory is labeled as the transition maneuver in figure 9. Once the transition maneuver is complete, the aircraft is rotated to the chosen angle of attack and descends at this constant angle.

Figure 10 presents descent parameters for descents with pull-up at constant angle of attack at various descent angles of attack. Figure 11 presents total heat load integrated

over the descent time interval as a function of cruise Mach number at a cruise dynamic pressure of 23.94 kPa (500 lb/ft^2) for several descent angles of attack.

Descents with pull-up at constant g-load.- The descent with pull-up at constant angle of attack described in the previous section may exceed structural load or heating constraints. To provide control of initial g-loads, a constant g-load pull-up transitional maneuver is employed. The actual descent portion of the trajectory is still performed at a constant angle of attack. As depicted in figure 12, a constant g-load is selected and the necessary angle-of-attack schedule is flown to maintain the constant g-load with decreasing velocity and increasing altitude. The pull-up is terminated at a preselected flight-path angle and the vehicle coasts at approximately zero lift and minimum drag until it reaches zero flight-path angle and maximum altitude. The flight-path angle at pull-up termination can then be iterated to provide equilibrium glide descents at various preselected angles of attack.

Figure 13 presents descent parameters as a function of time for a descent angle of attack of 24° and pull-up g-loads of 1.5, 2.0, and 3.0. Figure 14 presents total heat load as a function of cruise Mach number for a cruise dynamic pressure of 23.94 kPa (500 lb/ft^2) and a 2g pull-up transition maneuver at several descent angles of attack. The insert in figure 14 shows the ratio of total heat load to that for a 2g pull-up descent plotted against descent angle of attack for 1.5g and 3.0g pull-up descents.

Turning descents.- A turning descent may be necessary to provide lateral range, selection of a downrange landing site, and avoidance of geographical features. To provide a trade-off between turns, heat load, and angle-of-attack limitations, the descent with pull-up at constant angle of attack was modified to include turns at the conclusion of the transition maneuver. Figure 15 is a schematic of this type of descent. Figure 16(a) shows the descent parameters of a turning trajectory with an angle-of-attack limit of 24° and a maximum change in heading angle of 90°. The turn is a 60° roll-angle turn, or approximately a 2g turn. Figure 16(b) presents the parameters for a maximum change in heading angle of 180°. Lateral range as a function of downrange for turning descents over a range of descent angle of attack and cruise Mach number is presented in appendix B.

The total descent heat load as a function of cruise Mach number is presented in figure 17 for a 90° turning descent at several descent angles of attack. The insert in figure 17 shows the ratio of total descent heat load to that for a nonturning descent as a function of descent angle of attack for turning descents to heading angles of 90° and 180°. When the desired heading angle is reached, the aircraft is returned to zero roll and the angle of attack is changed to provide equilibrium flight. Since the lift coefficient will now be lower throughout the remainder of the descent, the total heat load will increase. Thus, the insert in figure 17 shows that the 90° turn, which reached its final heading angle earlier in the heat pulse, resulted in the higher heat load. This difference in heat pulse can

be seen by comparing the curves in figures 16(a) and 16(b) and noting that the heat pulse persists for an additional 70 sec for the 90° turn (fig. 16(a)).

Descents With Drag Brakes

Flat-plate drag brakes have been added to the nominal descent, the high-dynamic-pressure descent, and the high-lift-coefficient descent (descent with pull-up) at constant angle of attack. These descents are presented in figures 18 to 20. Drag-brake sizes considered were 8 and 16 percent of the reference area. The drag brakes are discussed in further detail in appendix C.

Figure 21 presents aircraft total heat load as a function of drag-brake size for the nominal, high-dynamic-pressure, and high-lift-coefficient (pull-up at constant angle of attack) descents. High-lift-coefficient descents at descent angles of attack of 8°, 16°, 24°, and 32° are presented on the left side of the figure. The right side compares three different types of descent. All the descents are from the standard cruise condition. The solid lines are aircraft heat loads for uncooled drag brakes (except for radiation cooling). The dashed lines are the sum of the aircraft and the drag brake heat loads at a cold-wall temperature T_w of 367 K.

DISCUSSION OF RESULTS

Comparison of Descent Types

A sample of the descent types discussed is shown in figure 22 as a plot of altitude against Mach number. Also plotted for reference are lines of constant dynamic pressure; these cover the practical range of aircraft operation from $q/q_r = 0.1$, which approaches the limitations of aerodynamic controls, to $q/q_r = 3$, after which heating rates and structural loads may become critical. It can be seen that the types of descents discussed essentially cover the aircraft operating spectrum.

To simply indicate trends, the total heat load, maximum heating rate, time to landing, time to end of heat pulse, and downrange are compared in the following paragraphs for descents from $M_c = 8$ and $q_r = 23.94$ kPa (500 lb/ft^2). Results are presented in relation to the nominal (cruise angle of attack) descent.

Total heat load.- Figure 23 presents the total heat load on the aircraft for each descent type relative to the total heat load for the nominal descent. The figure shows that if no drag brakes are available, any of the descents flown at high lift coefficient give a sizable reduction in heat load from that for the nominal descent. The high-lift-coefficient descent at $\alpha = 32^{\circ}$ provides the lowest heat load.

The high-lift-coefficient descents at $\alpha = 24^{\circ}$ indicate trends in total heat load for constant g pull-ups, 2g turns, and drag-brake size. Since changes in total heat load

are small, it is evident that the type of transition maneuver required to achieve a high-lift-coefficient condition has little effect on the total heat load. This trend is also observed at all other cruise Mach numbers.

Drag brakes are a potent means of reducing the total heat load for the nominal descent and the high-dynamic-pressure descent (fig. 23). The drag brakes are much less effective for the high-lift-coefficient descents because their contribution to the total drag becomes relatively small, and the drag brake deflection angle decreases. The decrease in drag brake effectiveness with increasing angle of attack is demonstrated on the left of figure 21. The right side of the figure indicates the large reductions in heat load for the low angle-of-attack descents as compared with the descent at $\alpha = 24^{\circ}$. The heat load which must be absorbed by the aircraft thermal protection system with and without the additional heat load due to the drag brakes is also shown.

It may be seen that the choice of best descent with drag brakes may depend on the type of drag-brake thermal protection, the angle-of-attack capability of the vehicle, and the drag-brake size available.

Maximum heating rate.- Figure 24 presents maximum heating rate at any point in the trajectory for the descents presented in figure 21. In every case except the high-dynamic-pressure descent, the maximum heating rate occurred at the end of cruise when the angle of attack was increased and/or the velocity was at maximum. The maximum heating rate for the high-dynamic-pressure descent occurs during the 2g portion of the pull-up maneuver (t = 50 sec, fig. 7). The least severe maximum occurs for the nominal descents. Note that high-lift-coefficient descents and high g-load pull-ups produce substantial increases in heating rate.

Relative time to landing.- Figure 25 presents the relative time to landing and makes apparent the reason for consideration of the high-dynamic-pressure descent. If the capability for a short descent time is necessary, it is obviously desirable to consider designing the vehicle to fly the high-dynamic-pressure descent. For thermal protection systems which depend heavily on high surface temperatures and the associated radiative heat loss, the high-dynamic-pressure descent, because of its shorter descent time, may also be attractive from the standpoint of total heat load to the aircraft.

Time to end of heat pulse.- Figure 26 shows time to the end of the heat pulse. The high-dynamic-pressure descent provides the shortest time to the end of heat pulse, but the descent with turns at $\phi = 60^{\circ}$ and $\psi = 180^{\circ}$ is a close competitor. The use of drag brakes reduces the time still further for the high-dynamic-pressure descent and provides the additional choice of the nominal (cruise angle of attack) descent.

Relative downrange.- Figure 27 presents relative downrange and shows that for no drag brakes, the descent with turns at $\phi = 60^{\circ}$ and $\psi = 180^{\circ}$ provides the shortest range and the descent at $\alpha = 8^{\circ}$ provides the longest range. The high-dynamic-pressure descent provides a short downrange for nonturning descents and the shortest downrange of any descent considered with the addition of large drag brakes. The addition of drag brakes also greatly shortens the range required for the nominal descent (descent at cruise angle of attack).

Gust Loads

In addition to the design parameters listed for each descent type, limitations of a more general nature, such as gust loads, will also affect the choice of descent type. Figure 28 is a repeat of figure 22 with an overlay of the effects of loads due to vertical gusts. Calculation details are contained in appendix D. The calculation method was taken from reference 7. The lines for constant g-load in figure 28 are in addition to any load currently being experienced by the vehicle. It is apparent from figure 28 that the only descent type necessitating consideration of gust loads is the high-dynamic-pressure descent.

CONCLUSIONS

The envelope of probable descent operating conditions for a hypersonic air-breathing research airplane has been examined. Descents selected included descents at cruise angle of attack, descents at high dynamic pressure, descents at high lift coefficient, descents with turns, and descents with drag brakes. These descents were parametrically exercised and compared from the standpoint of cold-wall (367 K) aircraft heat load. The following conclusions are made from the analysis:

1. For a cooled research aircraft without drag brakes, a descent at high angle of attack (high lift coefficient) results in low total heat loads with a long time to landing and a medium downrange. The total heat load is a weak function of the type of transition maneuver required to attain the high-lift-coefficient condition.

2. If drag brakes are not available, the high-dynamic-pressure descent provides a short time to landing, small heat pulse interval, and short downrange but gives the highest peak heating rates and total cold-wall heat loads.

3. Drag brakes are an effective means of reducing total heat load, range, and descent time, particularly for those descents which employ a low angle of attack.

4. With drag brakes, the choice of descent types available for reducing the total heat load is dependent on drag-brake size and the type of drag-brake thermal protection.

5. For overall requirements of low total heat load, low maximum heating rate, short time interval to landing, small heat pulse interval, and short downrange, an attractive choice is the descent at cruise angle of attack with large drag brakes.

6. Turning descents provide a decrease in heat pulse time, downrange, and time to landing compared with the no-turn descent, with a minimal penalty in total heat load.

Langley Research Center,
National Aeronautics and Space Administration,
Hampton Va., February 18, 1975.

APPENDIX A

VEHICLE AERODYNAMICS AND HEATING

Subsonic, transonic, and low supersonic aerodynamic characteristics for the vehicle shown in figure 1 were estimated by using the methods of reference 8. Hypersonic aerodynamics were calculated with the aid of the Hypersonic Arbitrary-Body Aerodynamic Computer Program (refs. 2 and 3). Tables I and II give C_L and C_D from these calculations for a range of Mach number and for angles of attack from -4^o to 18^o, and extrapolated data from 18 to 32^o.

The Hypersonic Arbitrary-Body Aerodynamic Computer Program (refs. 2 and 3) was employed with a suitable heat-transfer modification to calculate heating data. To simplify the calculations, the flow was assumed to be all turbulent, to be everywhere attached, and to have no component interactions. Since the primary interest was in an aluminum structure vehicle, wall temperature was assumed to be maintained constant at 367 K. The leading edges were assumed to be sharp.

To generate a meaningful distribution of the heating, the vehicle was divided into 200 sections, as shown in the three-view computer drawing in figure 2. The computer code was used to compute the local flow conditions at the center of each section and the Spalding-Chi relationships, modified to calculate Stanton number (ref. 4), were employed to determine the heating at the center point of each section. This heating rate was assumed to apply to the entire area of that particular section. The sections were then summed to generate the total vehicle heat load. The vehicle heating rates calculated are presented in figure 29 as a function of angle of attack for Mach numbers of 4, 6, 8, and 10 and dynamic pressure levels of 4.788, 23.94, 47.88, and 71.82 kPa (100, 500, 1000, and 1500 lb/ft^2).

APPENDIX B

LATERAL RANGE

Lateral range as a function of downrange for three heading angles of 0^{o}, 90^{o}, and 180^{o} are plotted in figure 30(a) for a descent angle of attack of 16^{o}, cruise Mach numbers of 6, 8, and 10 from a cruise dynamic pressure of 23.94 kPa (500 lb/ft^2). Information is given in the same manner for descent angle-of-attack values of 24^{o} and 32^{o} in figures 30(b) and 30(c). These plots allow a preliminary determination of landing footprint.

APPENDIX C

DRAG BRAKES

The drag-brakes are assumed to operate in free-stream flow, to be simple flat plates, and to make no significant changes in lift coefficient or pitching moment when deployed. The drag brakes are visualized as opening from the sides of the twin vertical tails (fig. 1) to an incidence angle with the flow of 30^{o}. As the vehicle angle of attack is increased, the effective angle of incidence decreases. In any practical case, this would probably cause lift and an associated pitching moment, but these effects have been ignored for this study.

Aerodynamics

Drag-brake aerodynamics were computed separately and the resulting drag increment was added to the vehicle drag for drag-brake sizes of $0.08S_R$ and $0.16S_R$. A sample of C_D for the vehicle alone and with drag brakes of $0.08S_R$ and $0.16S_R$ is shown in figure 31 as a function of angle of attack for a Mach number of 8. Table III presents C_D for a Mach number range for the vehicle with the two sizes of drag brakes.

Heating

Drag-brake heating was computed separately and is shown incrementally in order to compare it with the vehicle total heat load in figures 21 and 23 and with vehicle heating rate in figure 24. Assumptions for the heating calculations were a sharp leading edge, all turbulent flow, cold-wall $(T_W = 367\ K)$ conditions, and no heating on the lee side of the plate. The effective incidence angle of the plate with the flow was calculated as a function of vehicle angle of attack.

APPENDIX D

GUST LOAD CALCULATIONS

Gust loading due to vertical gusts were calculated as prescribed in reference 7. In the notation of reference 7, the load factor n due to gusts is expressed as

$$n = 1 + \frac{K_g U_{de} V a}{498(W/S)}$$

In this equation, the terms, their meaning, and their values for this particular case are as follows:

a	normal-force-coefficient slope, 1.08 radian^{-1}
$\bar{c}$	mean aerodynamic chord, 11.887 m (39 ft)
g	acceleration due to gravity, 9.8066 m/sec^2 (32.174 ft/sec^2)
K_g	gust alleviation factor, $\frac{0.88\mu_g}{5.3 + \mu_g}$
μ_g	airplane mass ratio, $\frac{2(W/S)}{\rho \bar{c} a g}$
U_{de}	derived gust velocities
V	airplane equivalent speed
W/S	wing loading, 1558.6 N/m^2 (32.55 lb/ft^2)
ρ	free-stream density

Values of U_{de} given in reference 7 are used to an altitude of 15.24 km and linearly extrapolated to zero velocity at approximately 24.38 km.

REFERENCES

1. Nagel, A. L.; and Becker, J. V.: Key Technology for Airbreathing Hypersonic Aircraft. AIAA Paper No. 73-58, Jan. 1973.

2. Gentry, Arvel E.: Hypersonic Arbitrary-Body Aerodynamic Computer Program (Mark III Version). Vol. I – User's Manual. Rep. DAC 61552, Vol. I (Air Force Contract Nos. F33615 67 C 1008 and F33615 67 C 1602), McDonnell Douglas Corp., Apr. 1968. (Available from DDC as AD 851 811.)

3. Gentry, Arvel E.; and Smyth, Douglas N.: Hypersonic Arbitrary-Body Aerodynamic Computer Program (Mark III Version). Vol. II – Program Formulation and Listings. Rep. DAC 61552, Vol. II (Air Force Contract Nos. F33615 67 C 1008 and F33615 67 C 1602), McDonnell Douglas Corp., Apr. 1968. (Available from DDC as 851 812.)

4. Neal, Luther, Jr.; and Bertram, Mitchel H.: Turbulent-Skin-Friction and Heat-Transfer Charts Adapted From the Spalding and Chi Method. NASA TN D-3969, 1967.

5. Baradell, Donald L.: Lateral Range Control by Banking During Initial Phases of Supercircular Reentries. NASA TN D-1511, 1962.

6. Becker, J. V.: Preliminary Studies of Manned Satellites – Winged Configurations. NACA Conference on High-Speed Aerodynamics – A Compilation of the Papers Presented. NASA TM X-67-369, 1958, pp. 45-58.

7. Airworthiness Standards: Transport Category Airplanes. FAR Pt. 25, FAA, Feb. 1, 1965.

8. USAF Stability and Control Datcom. Contracts AF 33(616)-6460 and F33615-71-C-1298, McDonnell Douglas Corp., Oct. 1960. (Revised Feb. 1972.)

TABLE I.- VALUES OF LIFT COEFFICIENT FOR THE AIRCRAFT FOR A RANGE OF ANGLE OF ATTACK AND MACH NUMBER

Angle of attack, deg	Lift coefficients at Mach numbers of –									
	0	0.8	1.0	1.2	2	3	4	6	8	10
-4	-0.1160	-0.1323	-0.1370	-0.1374	-0.1214	-0.0901	-0.0699	-0.0517	-0.0437	-0.0394
-2	-.0580	-.0723	-.0760	-.0766	-.0686	-.0517	-.0399	-.0292	-.0244	-.0219
0	.0000	-.0123	-.0150	-.0158	-.0158	-.0129	-.0095	-.0065	-.0052	-.0046
2	.0580	.0477	.0460	.0450	.0370	.0291	.0234	.0181	.0156	.0141
4	.1160	.1077	.1070	.1058	.0898	.0749	.0595	.0453	.0387	.0350
6	.1740	.1677	.1680	.1666	.1426	.1224	.0972	.0743	.0639	.0582
8	.2320	.2277	.2290	.2274	.1954	.1710	.1365	.1053	.0913	.0838
10	.2900	.2877	.2900	.2882	.2482	.2199	.1767	.1380	.1210	.1120
12	.3480	.3477	.3510	.3490	.3010	.2997	.2185	.1729	.1533	.1431
14	.4060	.4077	.4120	.4098	.3538	.3206	.2618	.2102	.1884	.1773
16	.4640	.4677	.4730	.4706	.4066	.3717	.3063	.2495	.2604	.2144
18	.5220	.5277	.5340	.5314	.4594	.4231	.3518	.2909	.2662	.2542
20	.5800	.5877	.5950	.5922	.5122	.4730	.3950	.3290	.3050	.2940
22	.6380	.6477	.6560	.6530	.5650	.5230	.4390	.3680	.3440	.3330
24	.6960	.7077	.7170	.7138	.6178	.5740	.4845	.4070	.3830	.3720
26	.7540	.7677	.7780	.7746	.6706	.6250	.5300	.4470	.4270	.4120
28	.8120	.8277	.8390	.8354	.7234	.6770	.5745	.4860	.4600	.4520
30	.8700	.8877	.9000	.8962	.7762	.7270	.6190	.5255	.5000	.4910
32	.9280	.9477	.9610	.9570	.8290	.7780	.6630	.5650	.5380	.5280

TABLE II.- VALUES OF DRAG COEFFICIENT FOR THE AIRCRAFT FOR A RANGE OF ANGLE OF ATTACK AND MACH NUMBER

Angle of attack, deg	Drag coefficients at Mach numbers of –									
	0	0.8	1.0	1.2	2	3	4	6	8	10
-4	0.01900	0.01992	0.02154	0.06658	0.04636	0.03818	0.02894	0.02051	0.01708	0.01531
-2	.01375	.01398	.01528	.06014	.04084	.03291	.02470	.01710	.01398	.01235
0	.01200	.01200	.01320	.05800	.03900	.03050	.02280	.01561	.01263	.01107
2	.01375	.01398	.01528	.06014	.04084	.03123	.02341	.01612	.01311	.01151
4	.01900	.01992	.02154	.06658	.04636	.03534	.02677	.01886	.01557	.01383
6	.02774	.02982	.03195	.07730	.05560	.04298	.03309	.02402	.02026	.01829
8	.04000	.04368	.04654	.09230	.06244	.05436	.04254	.03184	.02742	.02514
10	.05573	.06150	.06529	.11160	.08500	.06961	.05531	.04254	.03731	.03465
12	.07497	.08328	.08822	.13519	.10524	.08885	.07156	.05635	.05023	.04768
14	.09771	.10902	.11530	.16306	.12916	.11226	.09157	.07361	.06650	.06304
16	.12395	.13872	.14656	.19522	.15676	.14001	.11553	.09460	.08648	.08260
18	.15369	.17238	.18198	.23167	.18804	.17222	.14365	.11959	.11045	.10616
20	.18693	.21000	.22158	.27241	.22300	.20915	.17625	.14895	.13876	.13404
22	.22366	.25158	.26533	.31743	.26164	.25103	.21362	.18299	.17172	.16651
24	.26390	.29312	.31326	.36674	.30396	.29815	.25611	.22208	.20962	.20381
26	.30763	.34662	.36536	.42034	.34996	.35088	.30412	.26657	.25273	.24610
28	.35486	.40000	.42162	.47823	.39963	.40962	.35808	.31685	.30127	.29350
30	.40559	.45750	.48205	.54041	.45299	.47489	.41850	.37328	.35544	.34603
32	.45982	.51888	.54664	.60688	.51003	.54725	.48595	.43628	.41538	.40363

TABLE III.- VALUES OF DRAG COEFFICIENT FOR THE AIRCRAFT WITH DRAG BRAKES FOR A RANGE OF ANGLE OF ATTACK AND MACH NUMBER

(a) $S/S_R = 0.08$

Angle of attack, deg	Drag coefficients at Mach numbers of –									
	0	0.8	1.0	1.2	2	3	4	6	8	10
-4	0.0795	0.0748	0.1190	0.1190	0.0928	0.0777	0.0614	0.0483	0.0432	0.0407
-2	.0743	.0690	.1120	.1120	.0874	.0725	.0572	.0449	.0402	.0378
0	.0726	.0670	.1100	.1100	.0856	.0701	.0554	.0435	.0388	.0365
2	.0743	.0690	.1120	.1120	.0847	.0708	.0559	.0440	.0393	.0369
4	.0795	.0748	.1190	.1190	.0928	.0748	.0592	.0466	.0417	.0392
6	.0880	.0845	.1290	.1290	.1020	.0823	.0655	.0517	.0463	.0436
8	.1000	.0982	.1440	.1440	.1150	.0935	.0748	.0594	.0534	.0503
10	.1150	.1160	.1630	.1630	.1310	.1090	.0874	.0700	.0631	.0597
12	.1340	.1370	.1860	.1860	.1510	.1280	.1030	.0836	.0759	.0721
14	.1570	.1620	.2140	.2140	.1740	.1510	.1230	.1010	.0919	.0887
16	.1820	.1920	.2450	.2450	.2020	.1780	.1470	.1210	.1120	.1070
18	.2110	.2250	.2810	.2810	.2320	.2100	.1750	.1460	.1350	.1300
20	.2440	.2620	.3210	.3210	.2670	.2460	.2070	.1750	.1630	.1580
22	.2800	.3030	.3660	.3660	.3050	.2880	.2440	.2090	.1960	.1900
24	.3190	.3430	.4140	.4140	.3470	.3340	.2860	.2480	.2340	.2270
26	.3620	.3960	.4670	.4670	.3920	.3860	.3330	.2920	.2760	.2690
28	.4080	.4490	.5240	.5240	.4410	.4450	.3870	.3410	.3240	.3160
30	.4580	.5050	.5860	.5860	.4930	.5090	.4470	.3970	.3780	.3680
32	.5110	.5660	.6510	.6510	.5500	.5810	.5140	.4600	.4380	.4250

TABLE III.- VALUES OF DRAG COEFFICIENT FOR THE AIRCRAFT WITH DRAG BRAKES FOR A RANGE OF ANGLE OF ATTACK AND MACH NUMBER – Concluded

(b) $S/S_R = 0.16$

Angle of attack, deg	Drag coefficients at Mach numbers of –									
	0	0.8	1.0	1.2	2	3	4	6	8	10
-4	0.1400	0.1300	0.1290	0.1710	0.1390	0.1170	0.0939	0.0761	0.0694	0.0661
-2	.1350	.1240	.1220	.1640	.1340	.1120	.0898	.0728	.0663	.0632
0	.1330	.1220	.1200	.1620	.1320	.1100	.0879	.0713	.0650	.0619
2	.1350	.1240	.1220	.1640	.1340	.1100	.0885	.0718	.0655	.0624
4	.1400	.1300	.1290	.1710	.1390	.1140	.0917	.0744	.0678	.0646
6	.1480	.1390	.1390	.1810	.1480	.1220	.0978	.0794	.0724	.0689
8	.1600	.1530	.1530	.1960	.1610	.1330	.1070	.0870	.0793	.0755
10	.1750	.1700	.1710	.2140	.1770	.1480	.1190	.0974	.0889	.0848
12	.1940	.1910	.1930	.2370	.1960	.1660	.1350	.1110	.1010	.0969
14	.2150	.2160	.2190	.2640	.2200	.1890	.1550	.1280	.1170	.1120
16	.2410	.2440	.2500	.2960	.2460	.2160	.1780	.1480	.1370	.1320
18	.2690	.2770	.2840	.3310	.2770	.2470	.2060	.1730	.1600	.1550
20	.3010	.3130	.3220	.3710	.3110	.2840	.2370	.2010	.1880	.1820
22	.3360	.3540	.3650	.4140	.3480	.3240	.2740	.2350	.2200	.2140
24	.2750	.3940	.4110	.4620	.3890	.3700	.3160	.2730	.2570	.2500
26	.4170	.4460	.4620	.5140	.4340	.4220	.3630	.3170	.3000	.2920
28	.4620	.4970	.5160	.5700	.4820	.4800	.4160	.3660	.3480	.3380
30	.5110	.5530	.5750	.6310	.5340	.5430	.4750	.4220	.4010	.3900
32	.5630	.6120	.6380	.6950	.5890	.6140	.5410	.4840	.4600	.4470

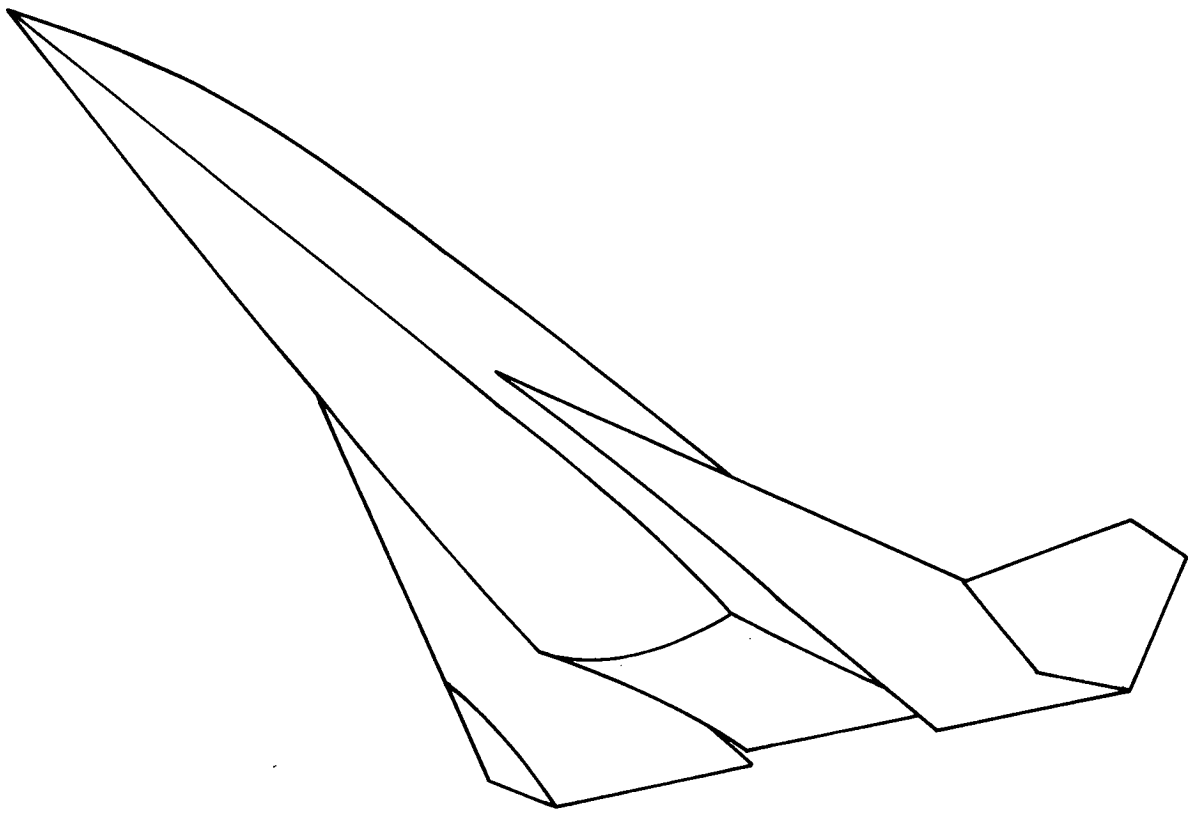

Figure 1.- Sketch of hypersonic research aircraft.

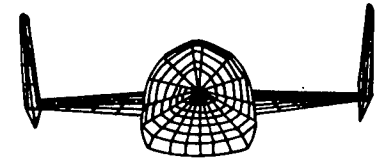

Reference area, 99.89 m^2
Operating weight empty, 15 876 kg
Fuselage length, 24.38 m

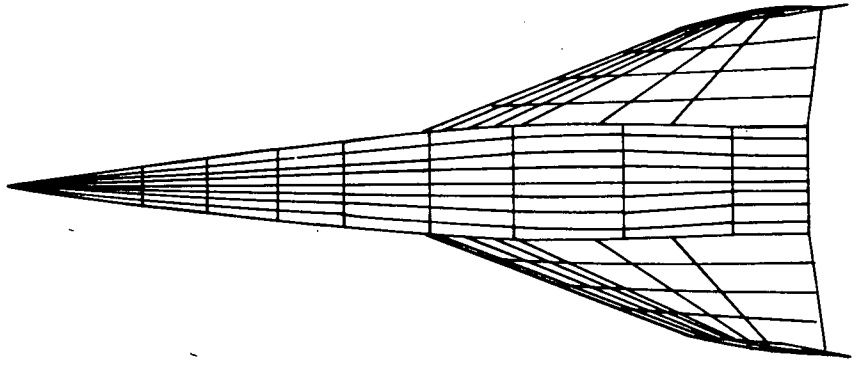

Figure 2.- Three-view computer drawing of the hypersonic research aircraft.

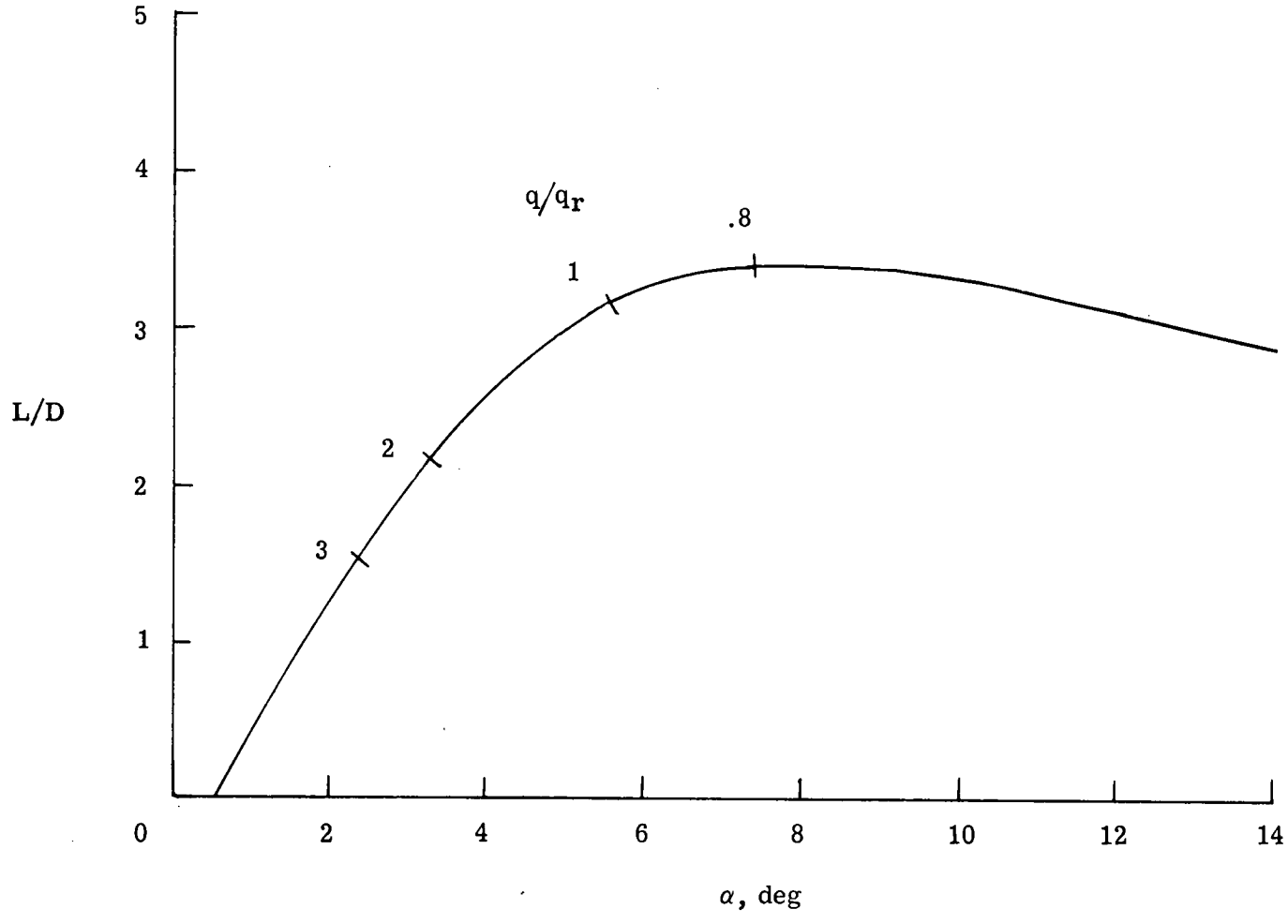

Figure 3.- Lift-drag ratio as a function of angle of attack.

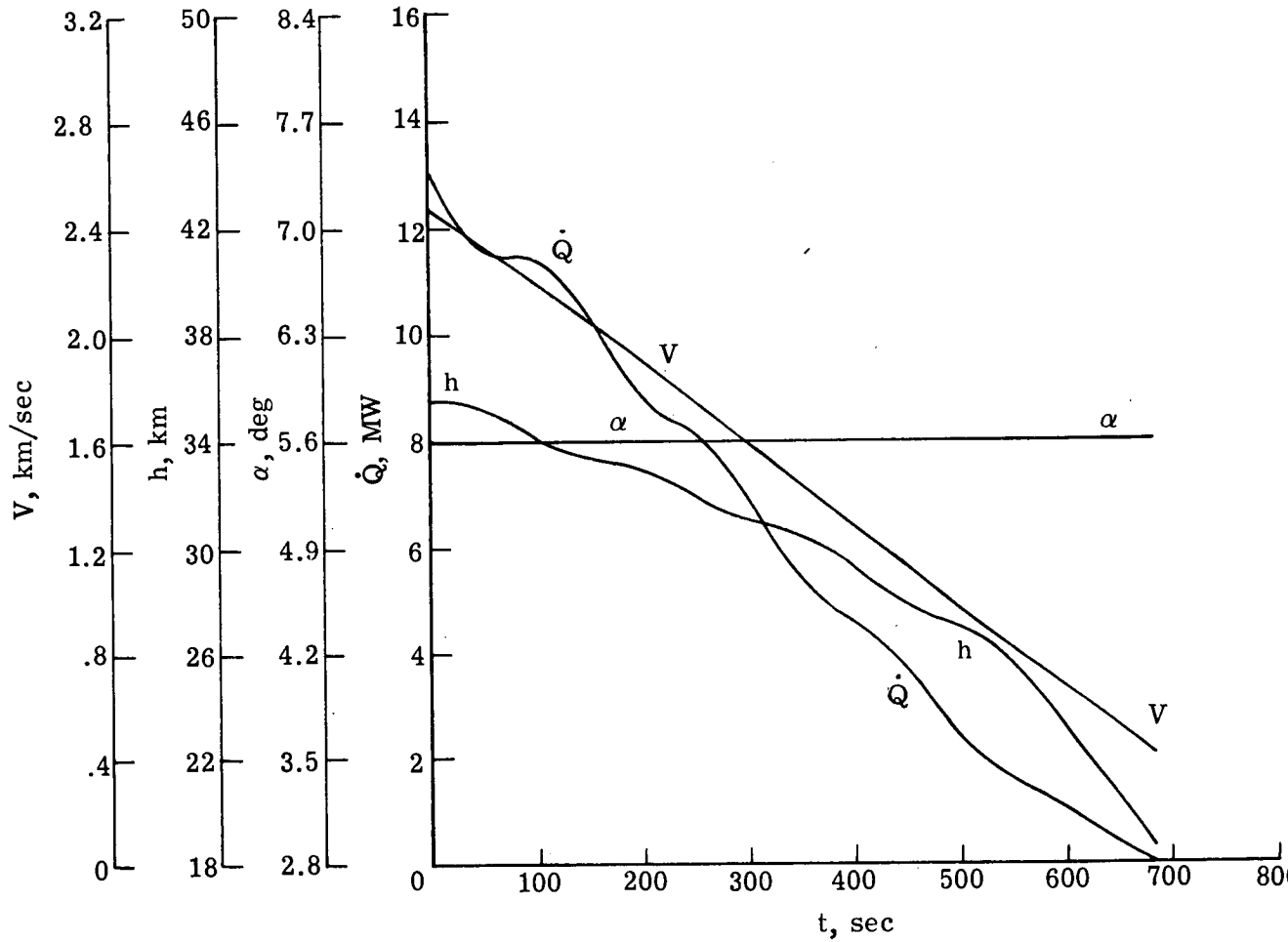

Figure 4.- Example of nominal descent parameters (descent at cruise angle of attack).

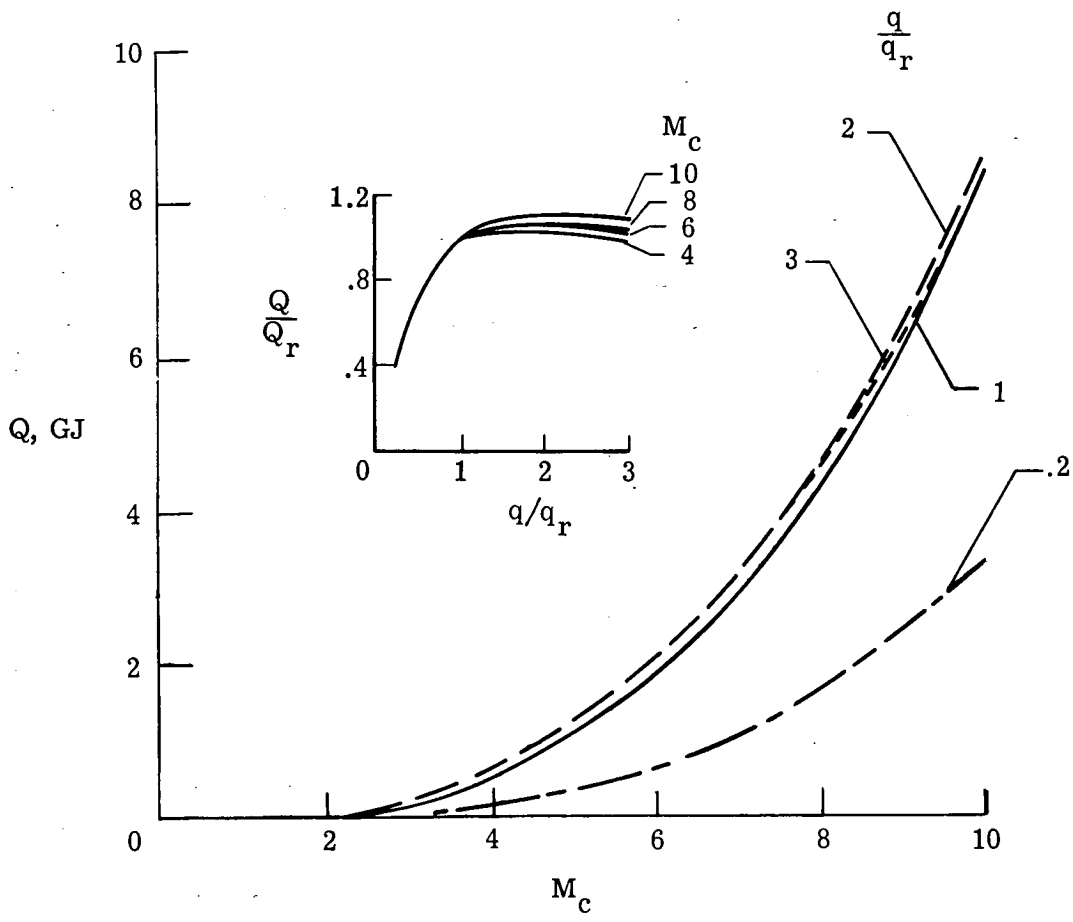

Figure 5.- Variation of descent heat load with cruise Mach number at dynamic pressure ratios of 0.2, 1, 2, and 3.

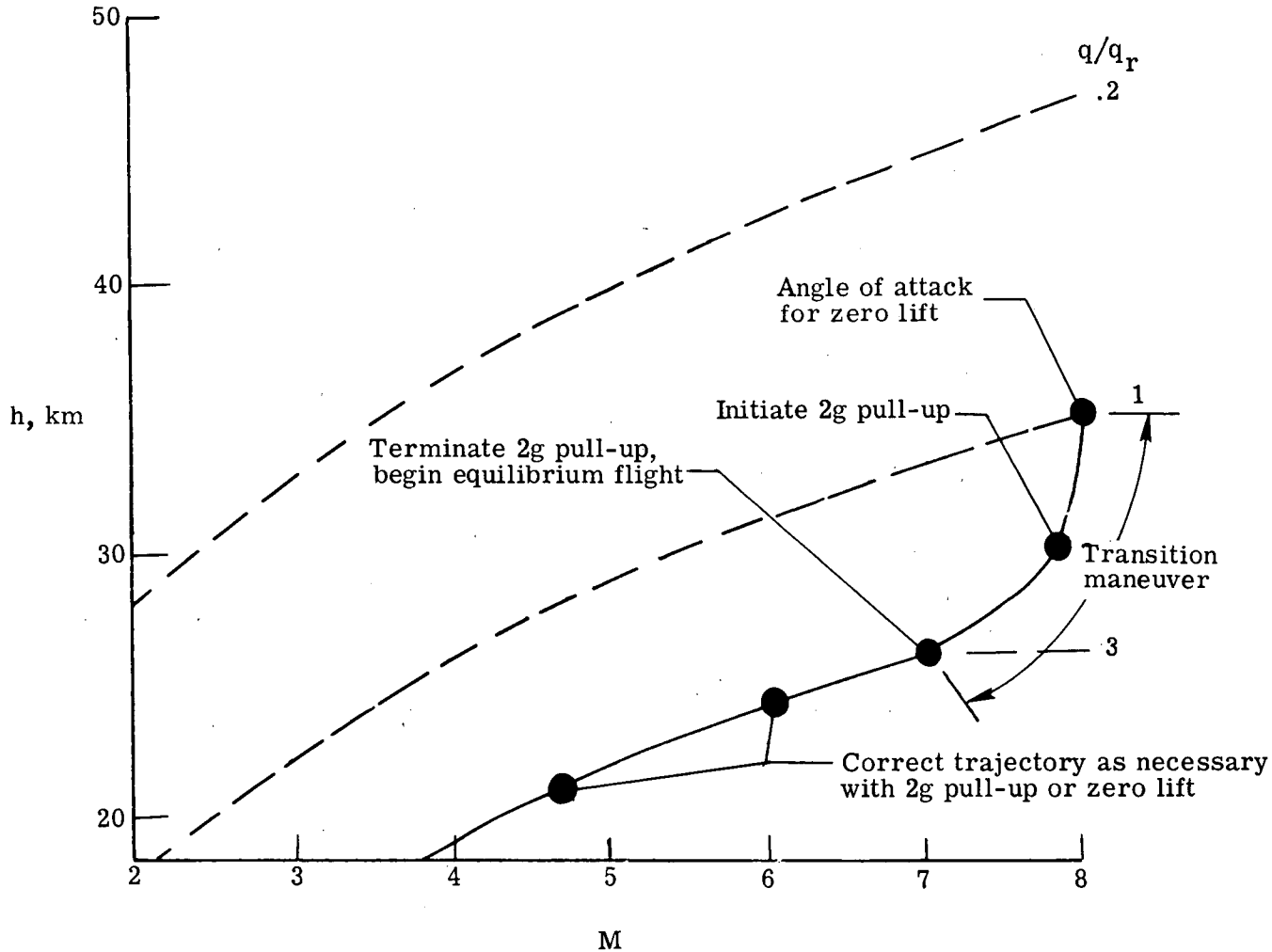

Figure 6.- Schematic explanation of the high-dynamic-pressure descent.

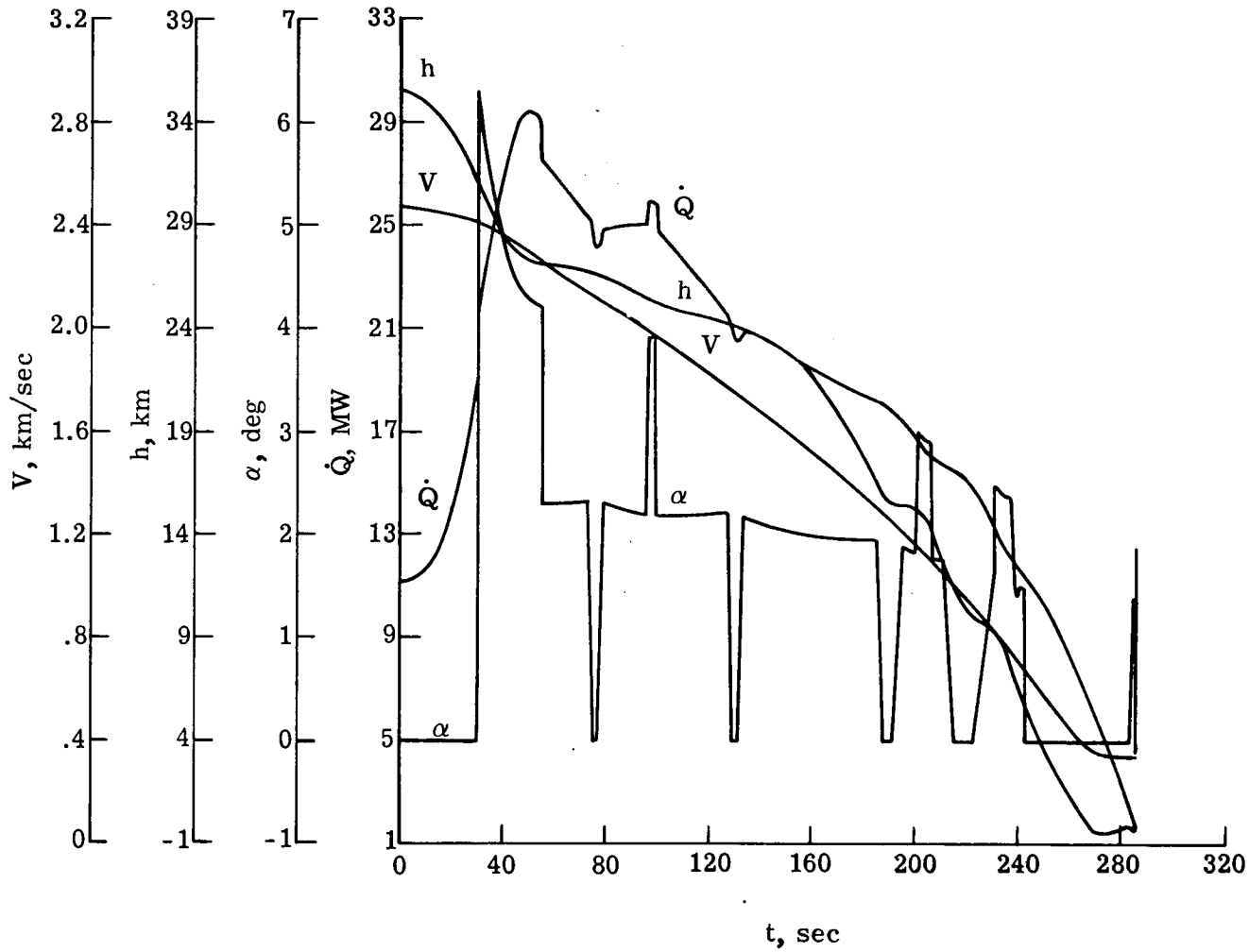

Figure 7.- High-dynamic-pressure descent at 71.82 kPa (1500 lb/ft^2) from the reference cruise condition.

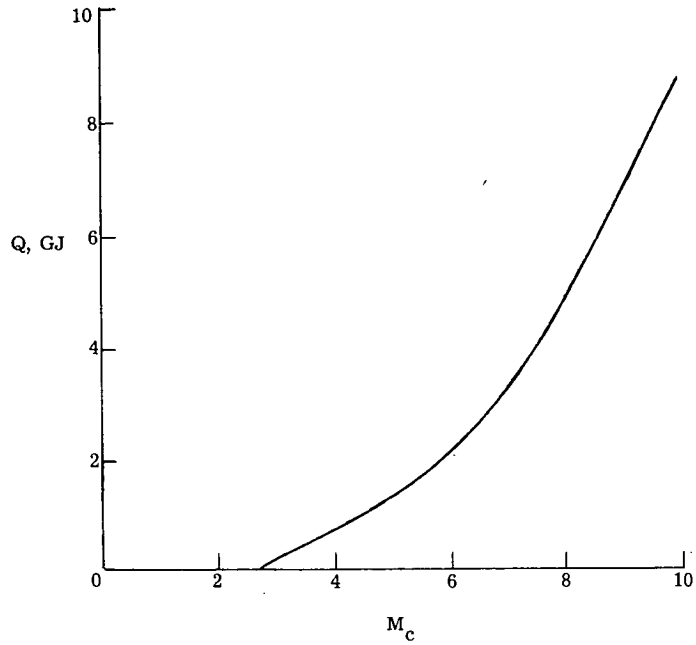

Figure 8.- Variation of total heat load with cruise Mach number for high-dynamic-pressure descent at 71.82 kPa (1500 lb/ft^2).

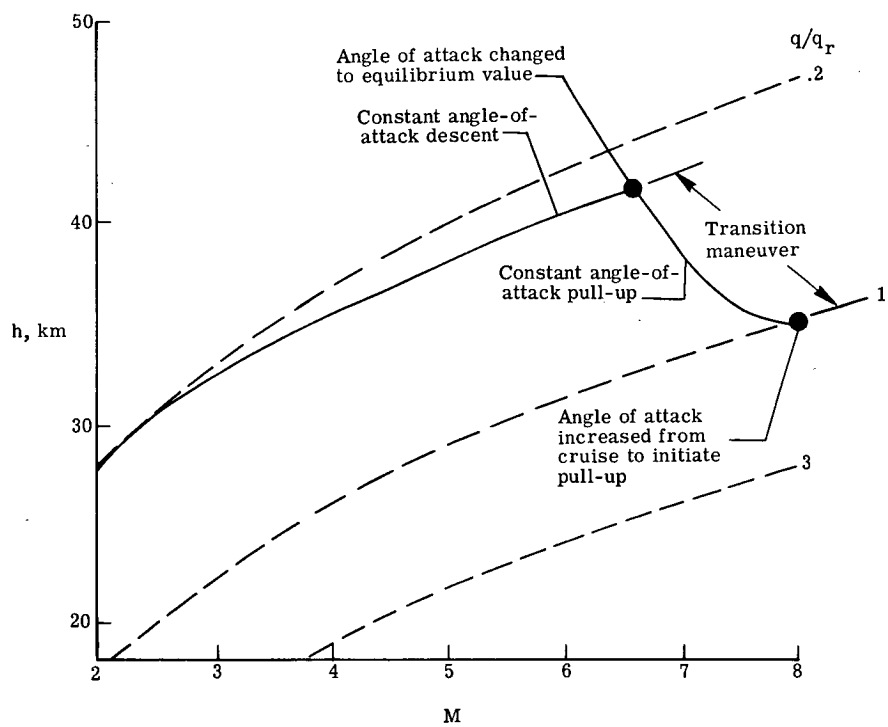

Figure 9.- Schematic explanation of descent with pull-up at constant angle of attack.

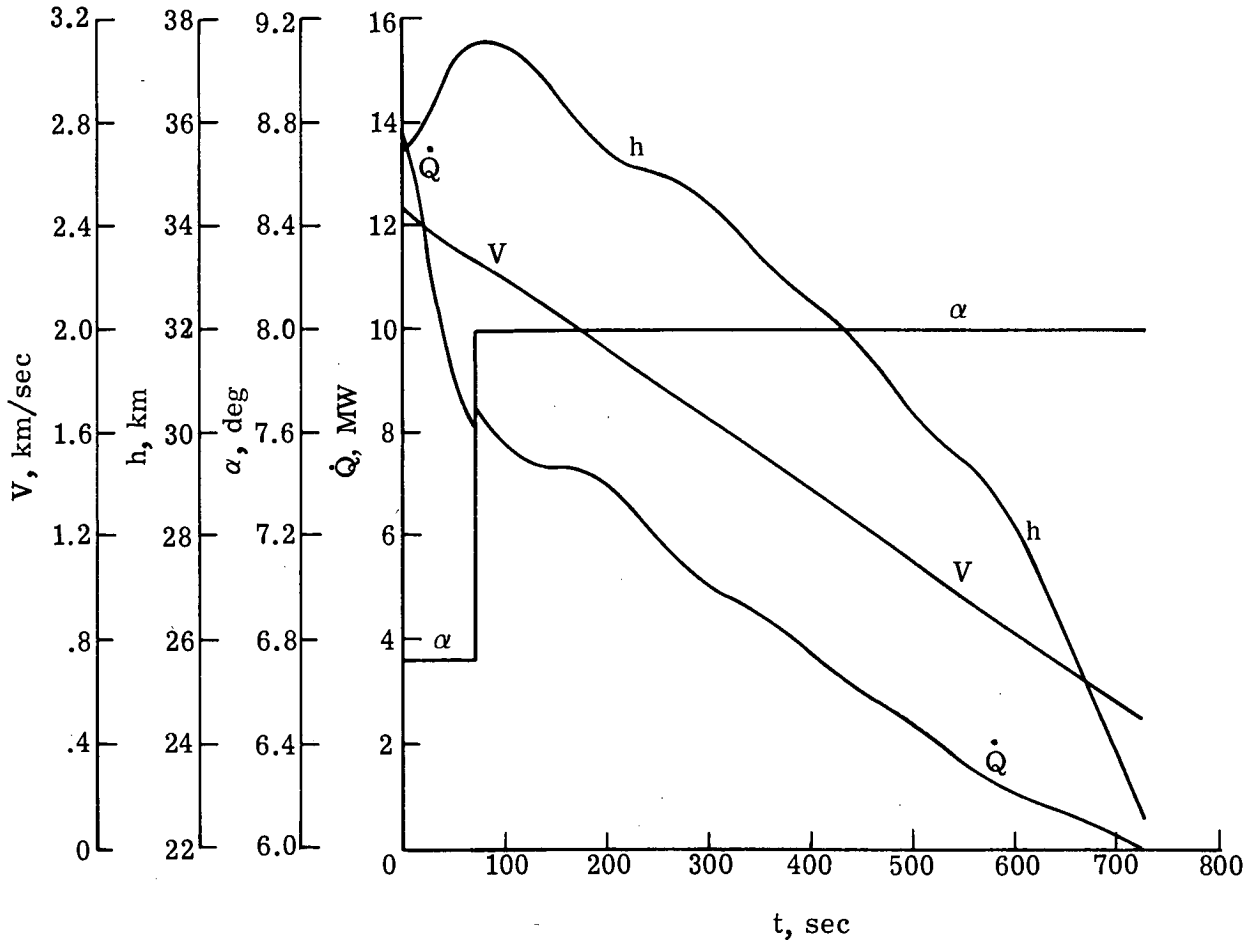

(a) $\alpha = 8^{o}$.

Figure 10.- Descent with pull-up at constant angle of attack for various descent angles of attack. $M_c = 8$; $q_r = 23.94$ kPa (500 lb/ft^2).

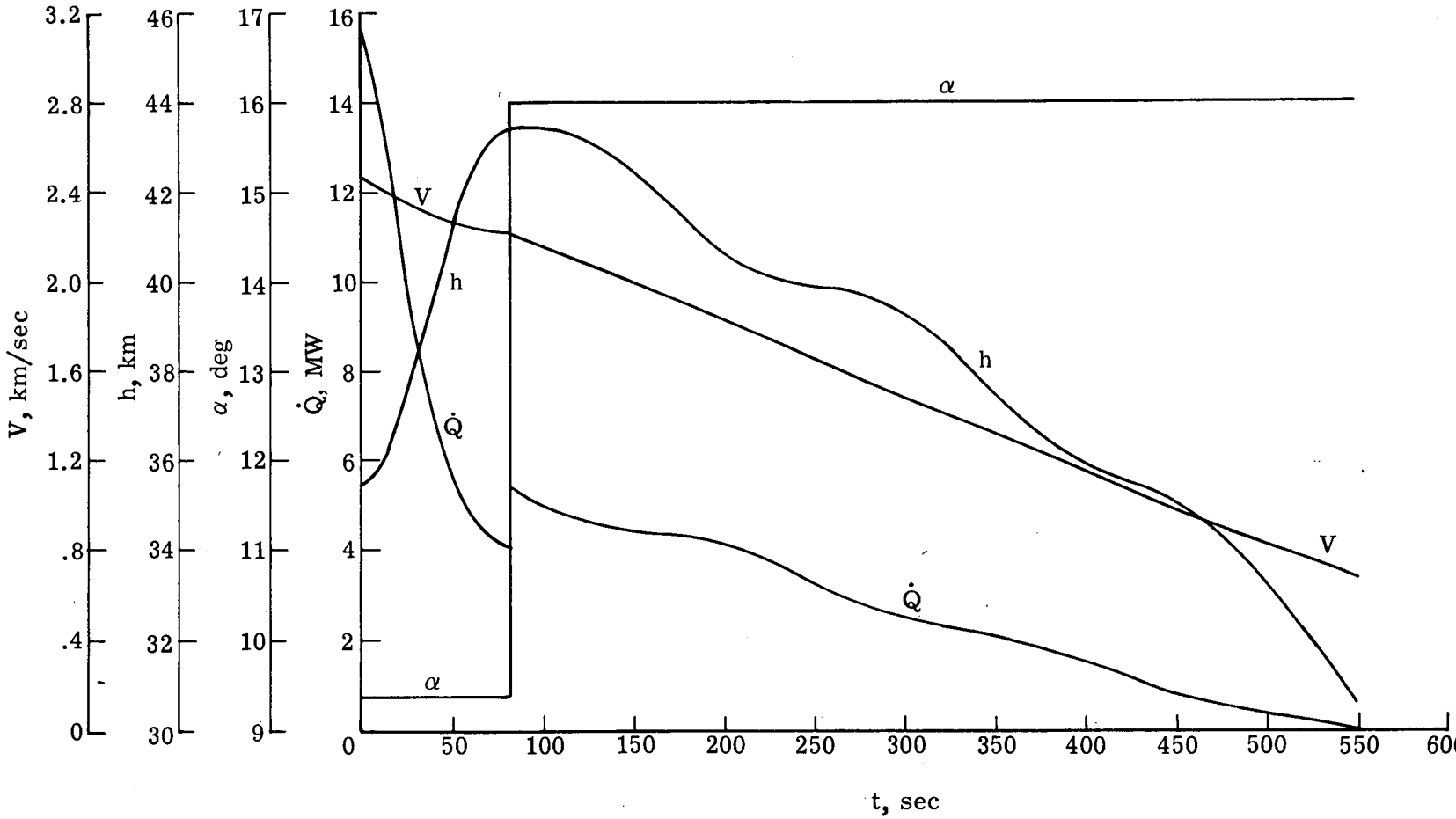

(b) $\alpha = 16^{o}$.

Figure 10.- Continued.

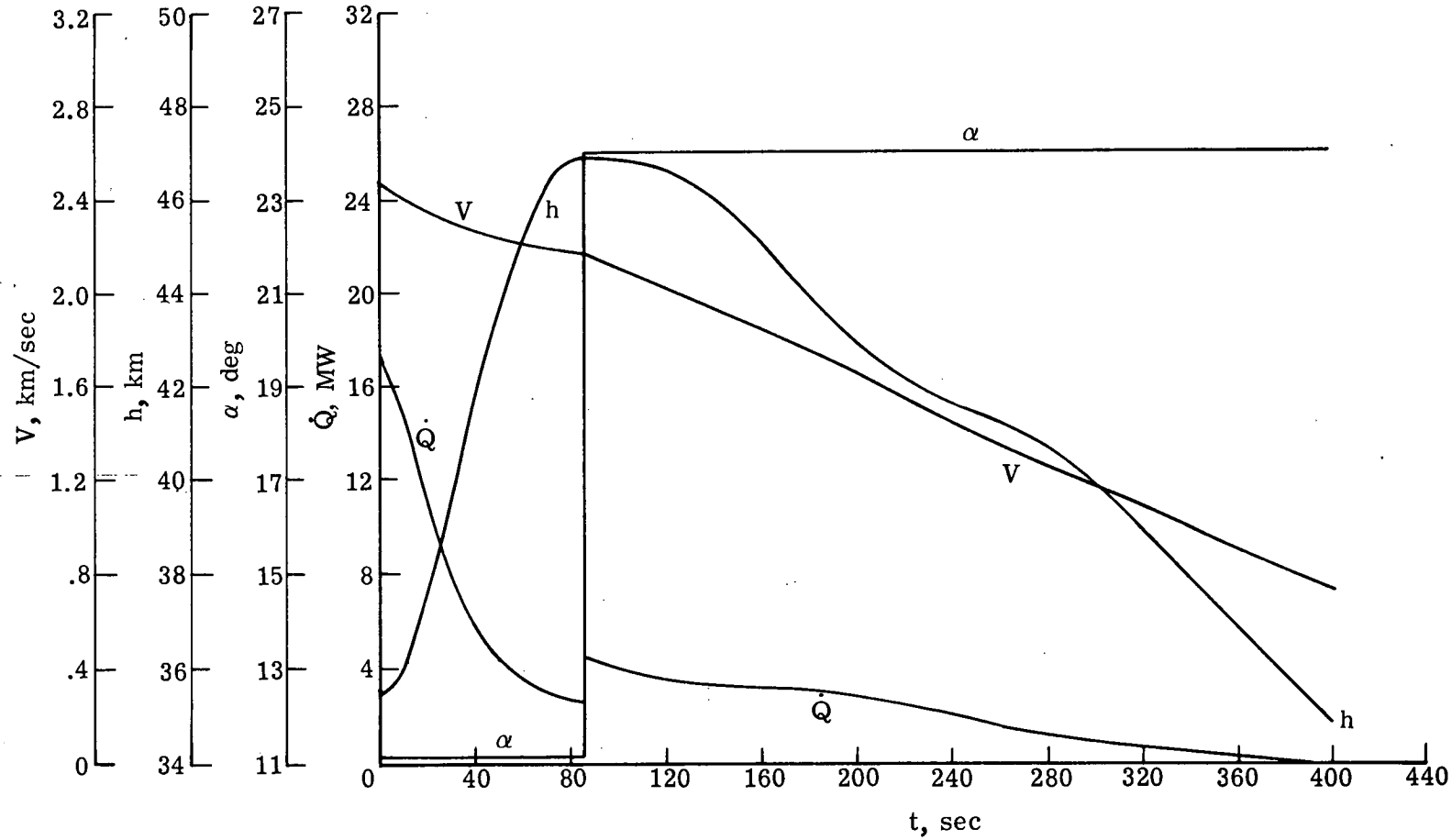

(c) $\alpha = 24^{o}$.

Figure 10.- Continued.

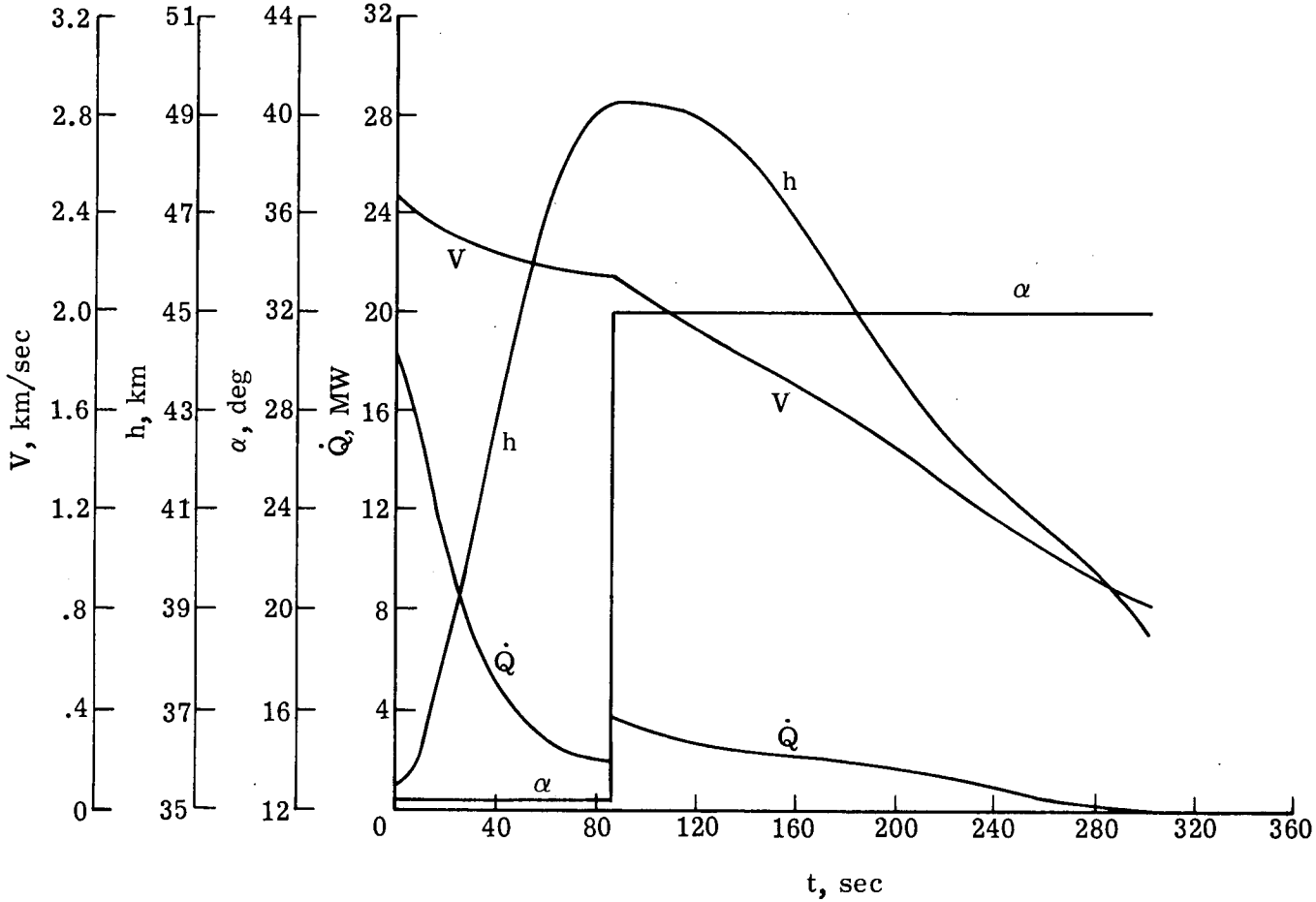

(d) $\alpha = 32^{o}$.

Figure 10.- Concluded.

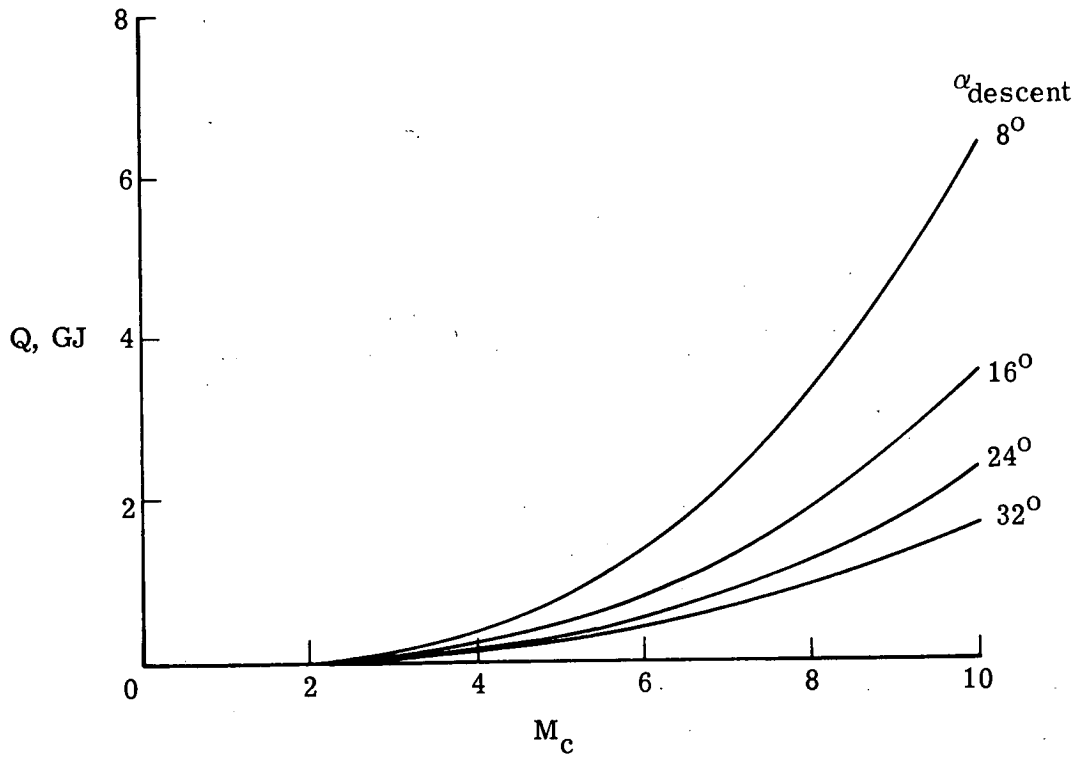

Figure 11.- Variation of total heat load with cruise Mach number for several descents at constant angle of attack. q_r = 23.94 kPa (500 lb/ft^2).

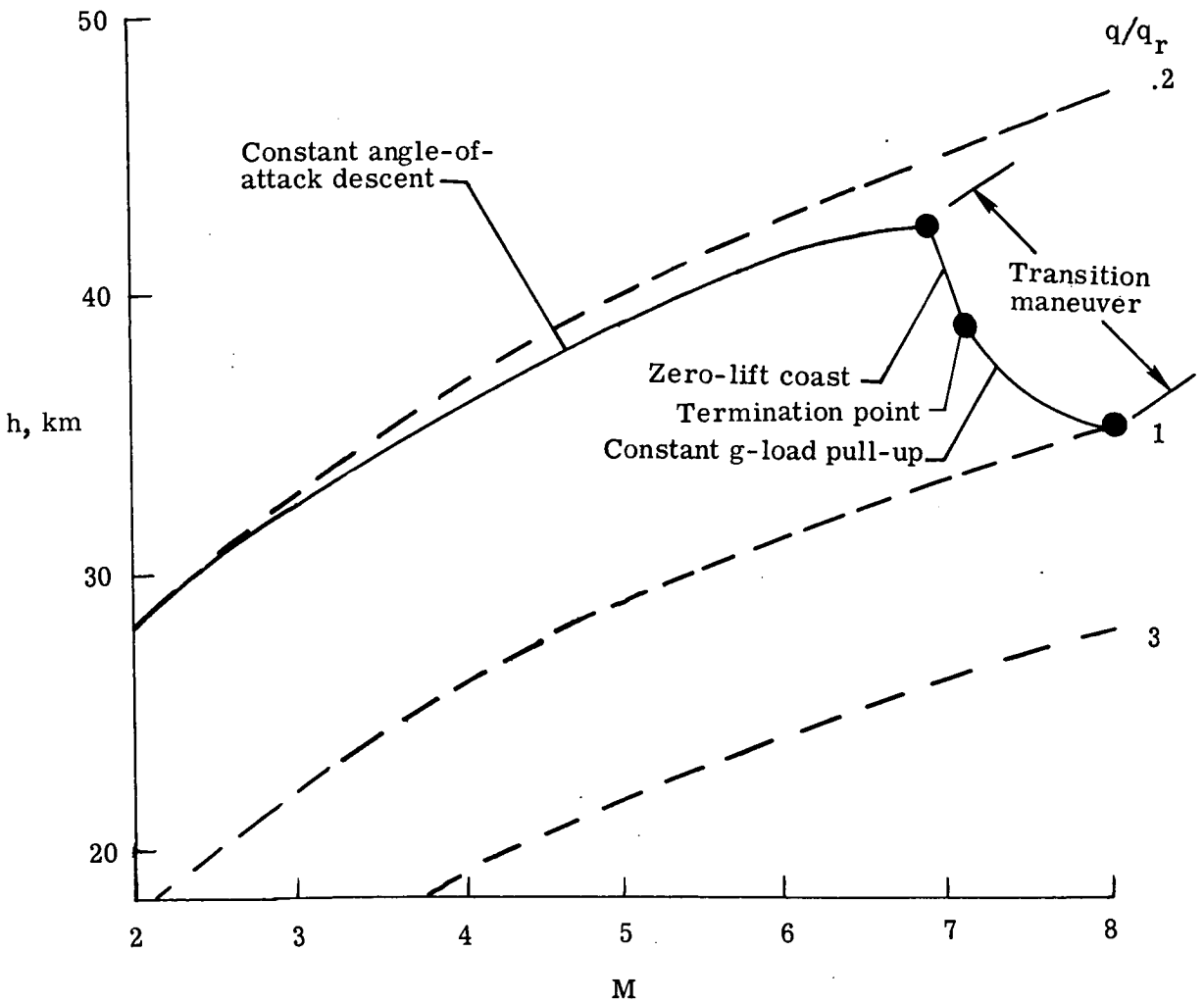

Figure 12.- Schematic explanation of descent with constant g-load pull-up.

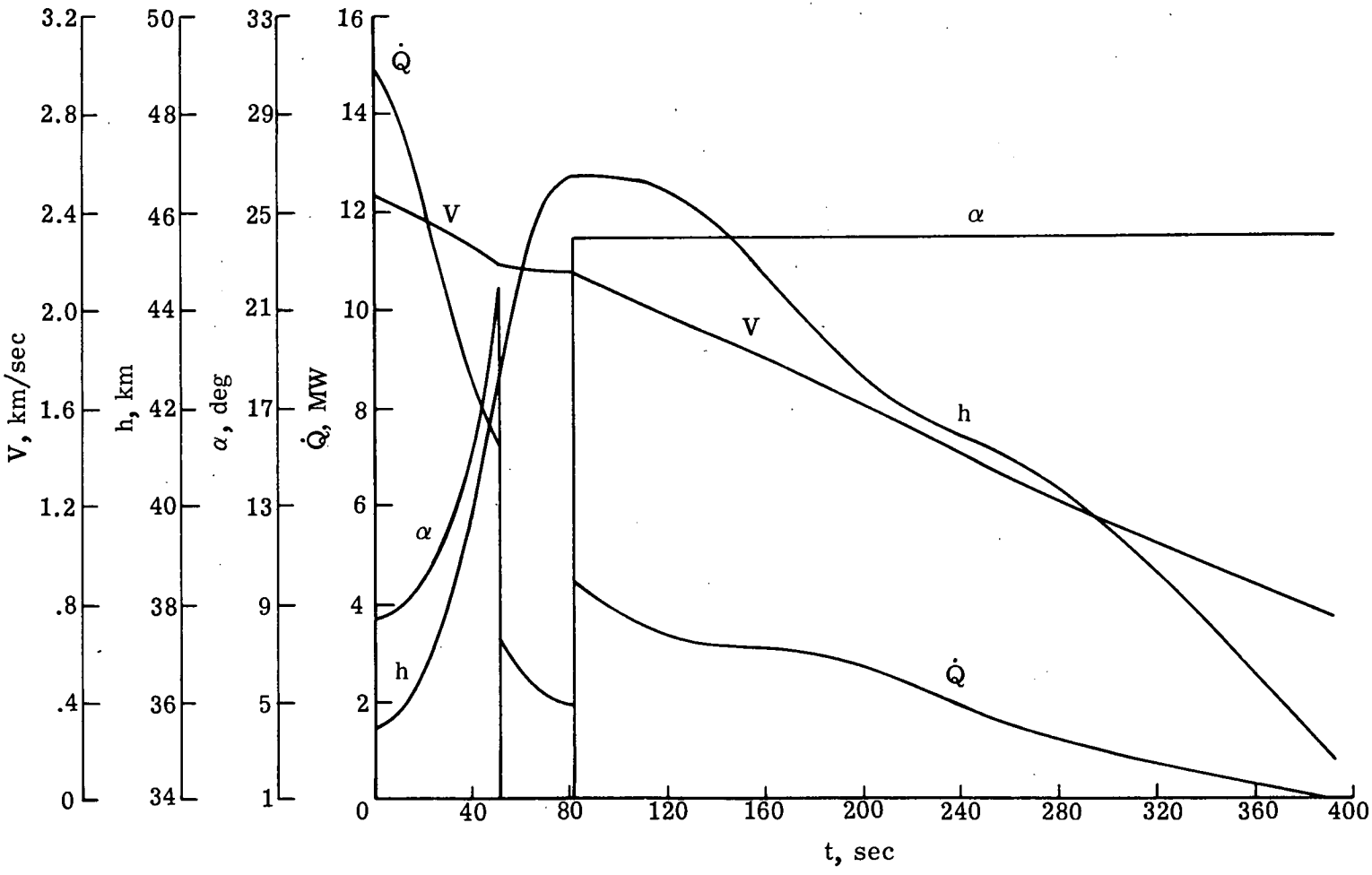

(a) 1.5g.

Figure 13.- Descents at descent angle of attack of 24° and pull-up g-loads of 1.5, 2.0, and 3.0.

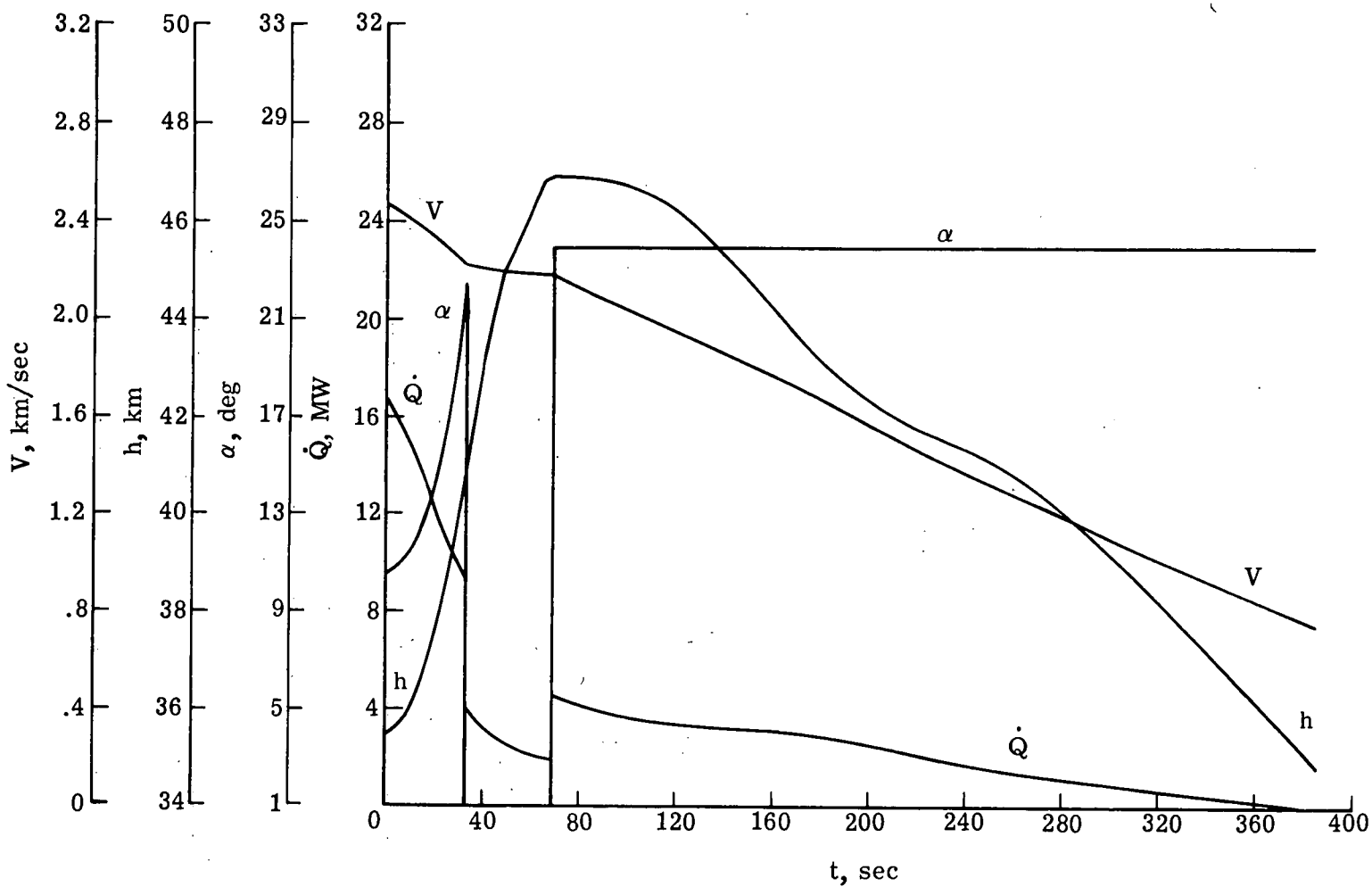

(b) 2.0g.

Figure 13.- Continued.

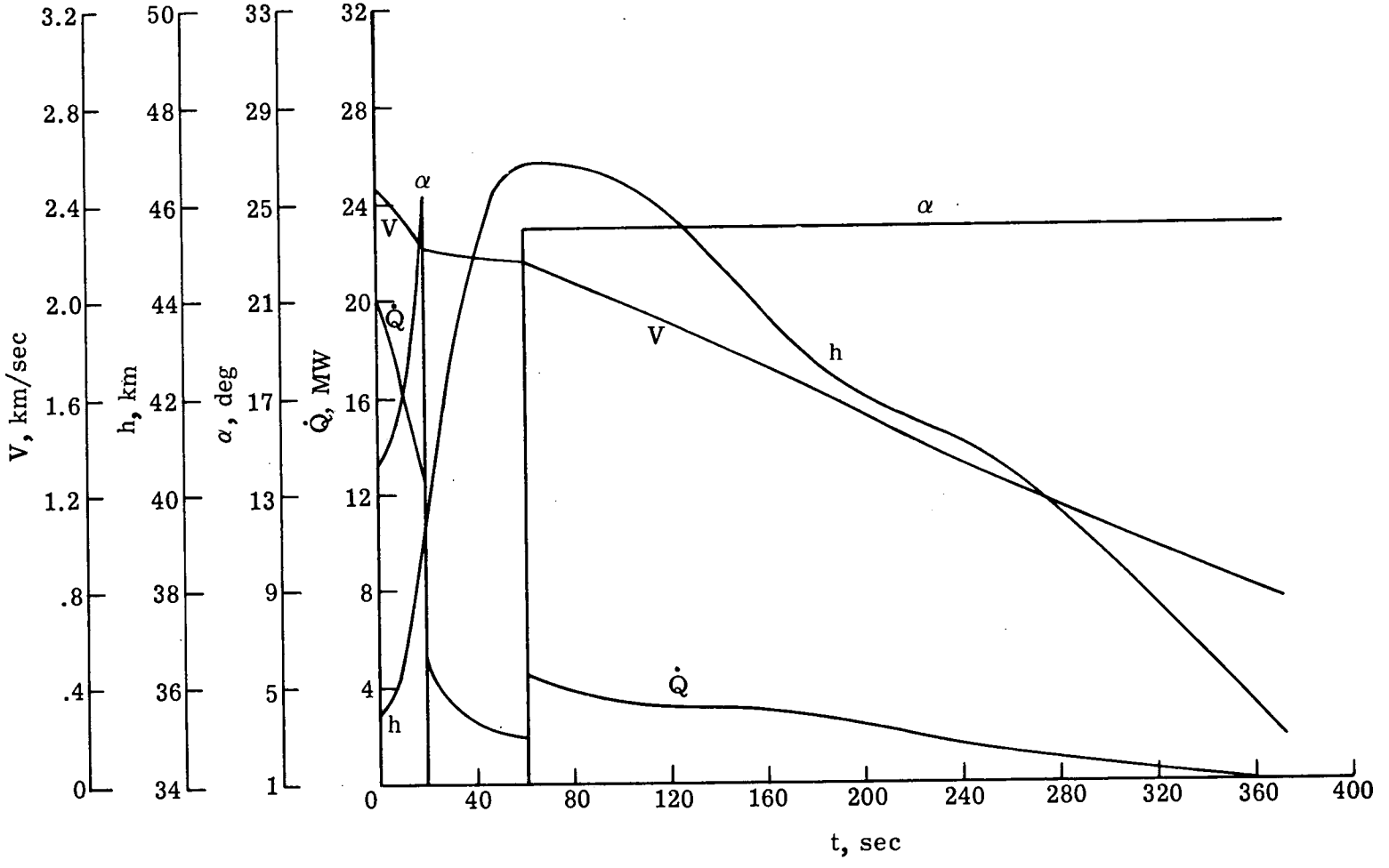

(c) 3.0g.

Figure 13.- Concluded.

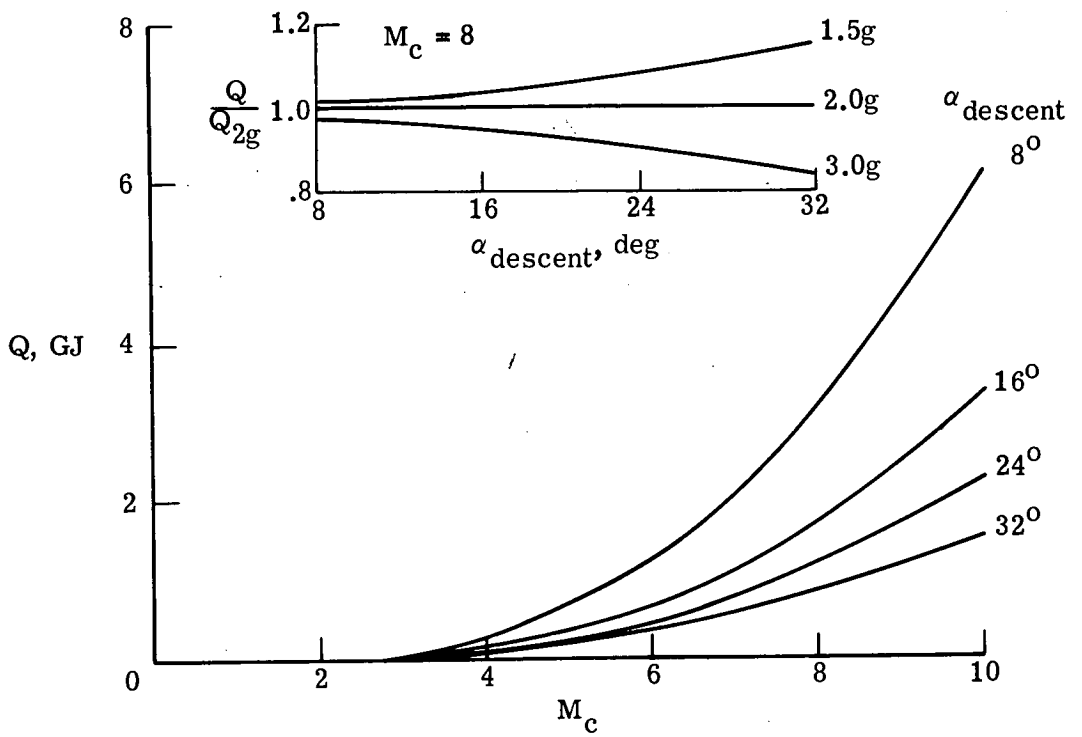

Figure 14.- Variation of total heat load with cruise Mach number for a constant 2g transition maneuver at several descent angles of attack. q_r = 23.94 kPa (500 lb/ft^2).

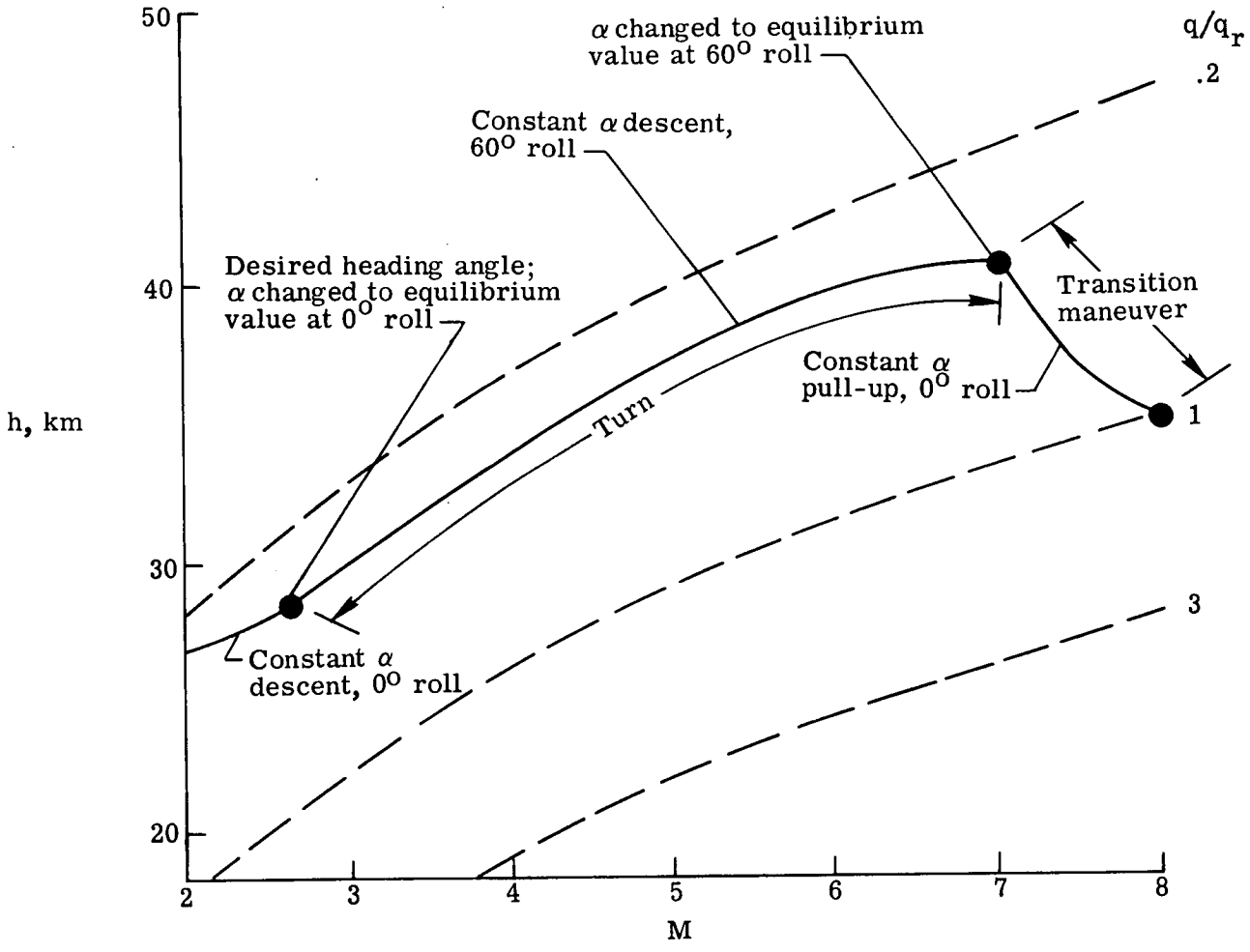

Figure 15.- Schematic explanation of the turning descent.

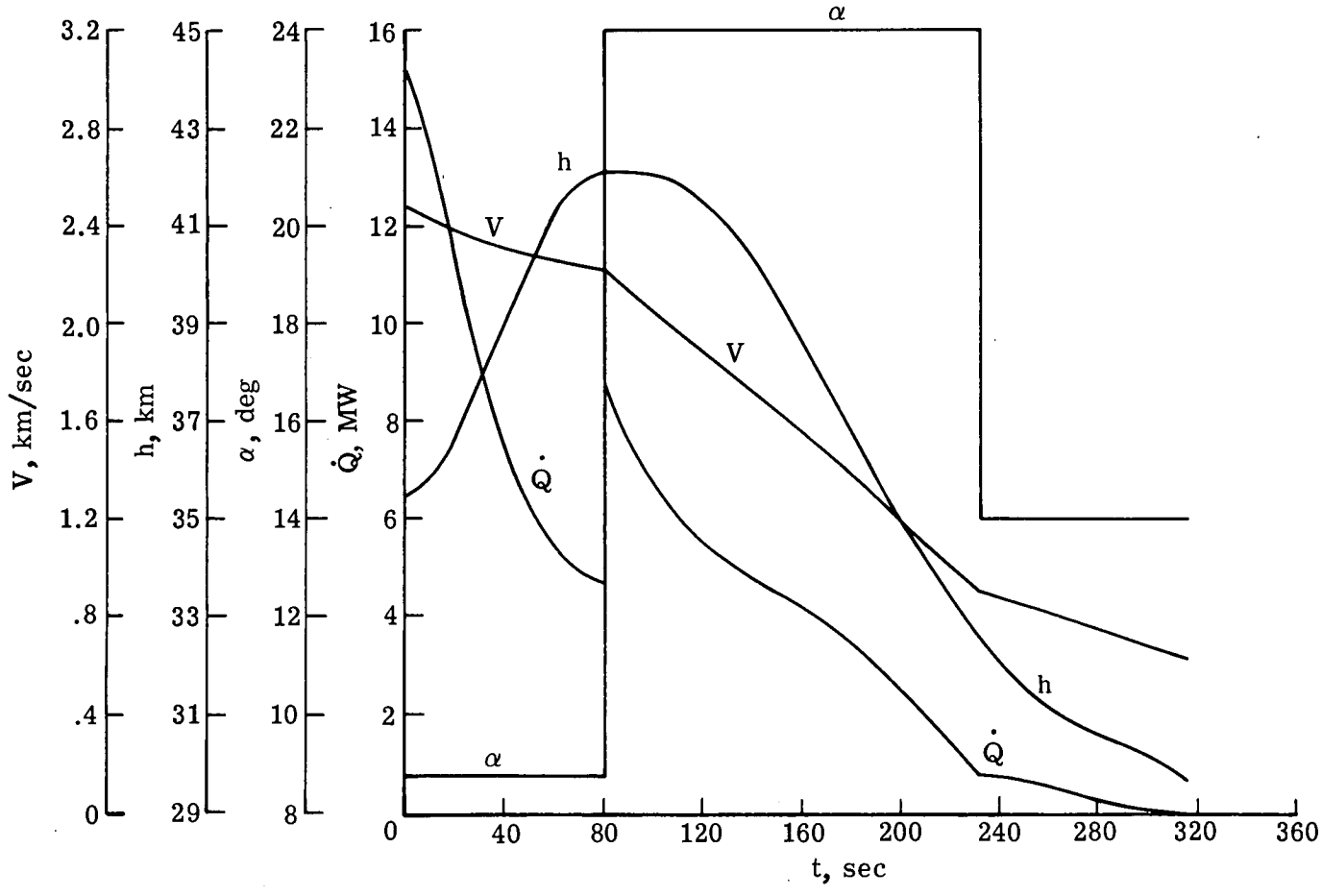

(a) $\psi = 90^{o}$.

Figure 16.- Turning descent for a 2g turn.

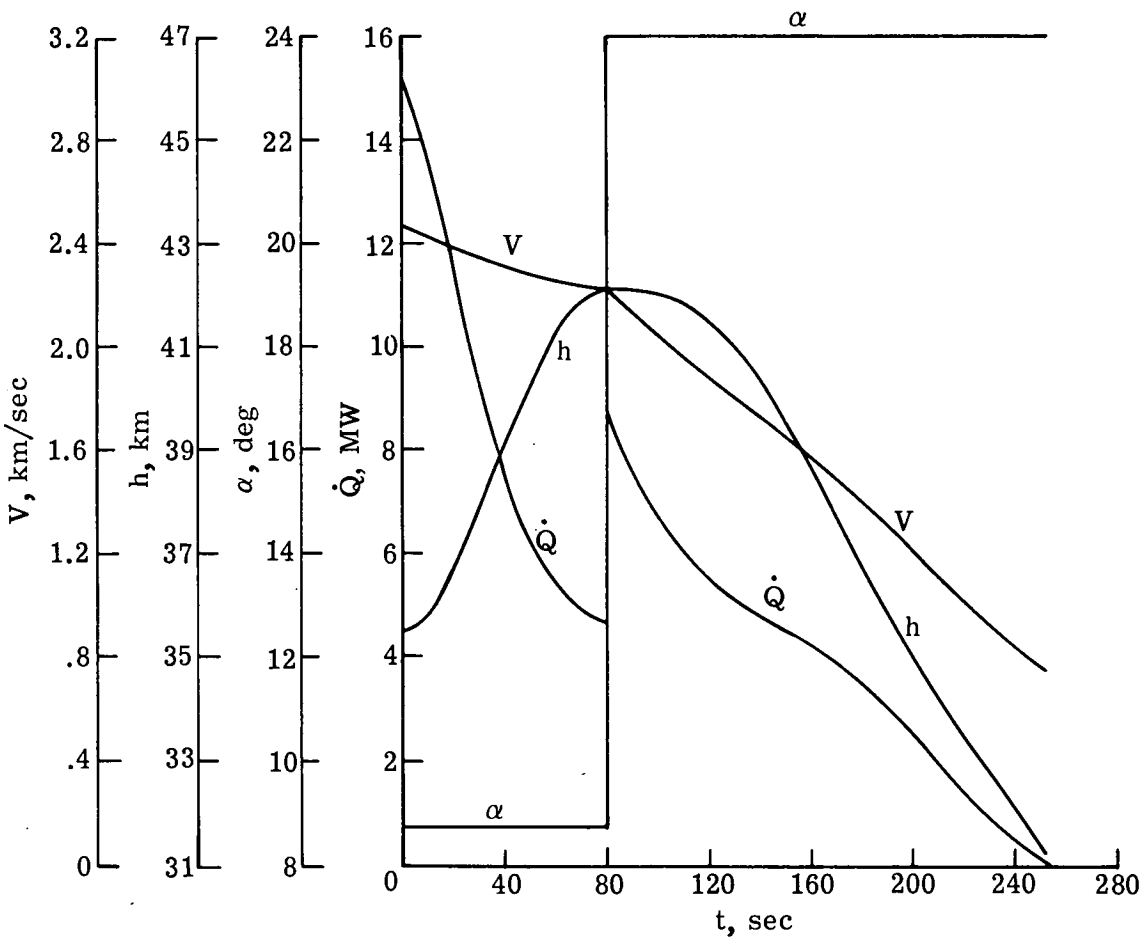

(b) $\psi = 180^{o}$.

Figure 16.- Concluded.

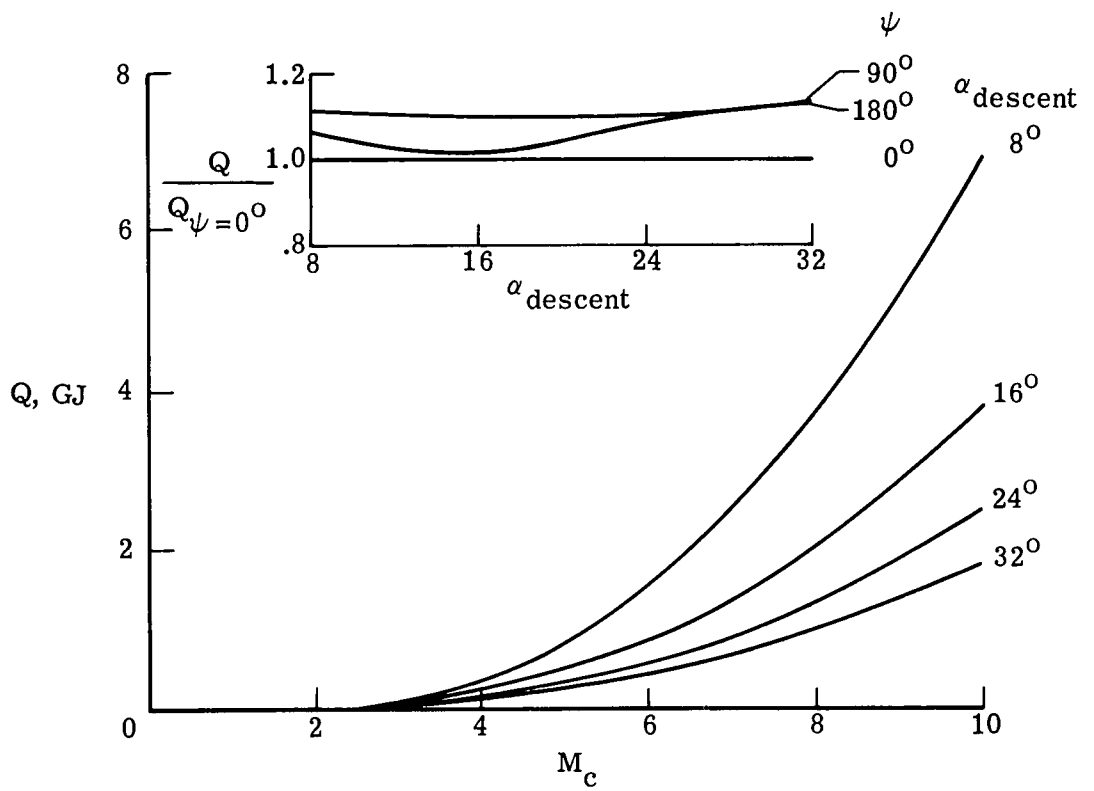

Figure 17.- Variation of total heat load with cruise Mach number for a heading angle of 90^{o} at several descent angles of attack. q_r = 23.94 kPa (500 lb/ft^2); $\phi = 60^{o}$.

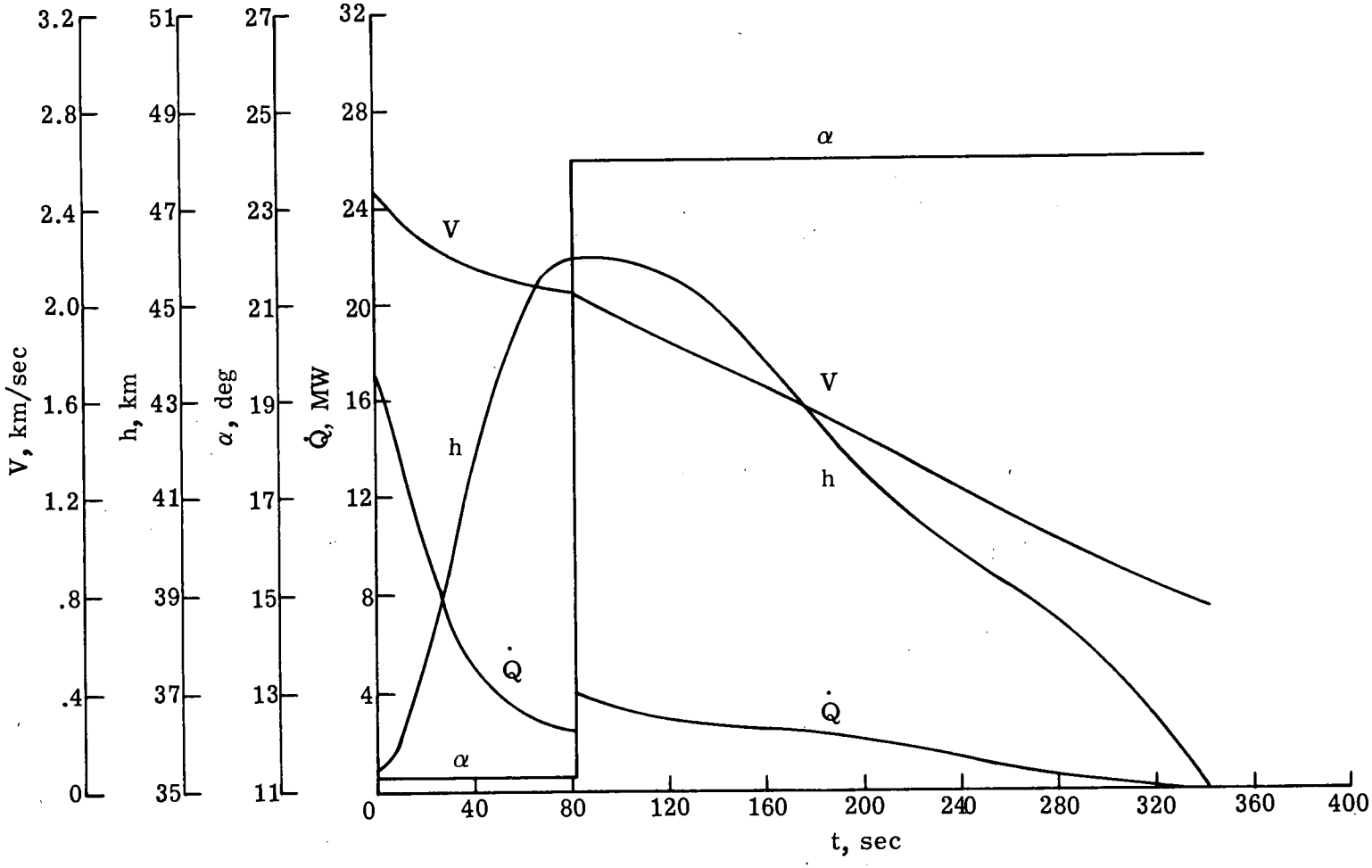

(a) $S/S_R = 0.08$.

Figure 18.- Drag brakes added to descent with pull-up at constant α and a descent angle of attack of 24^o.

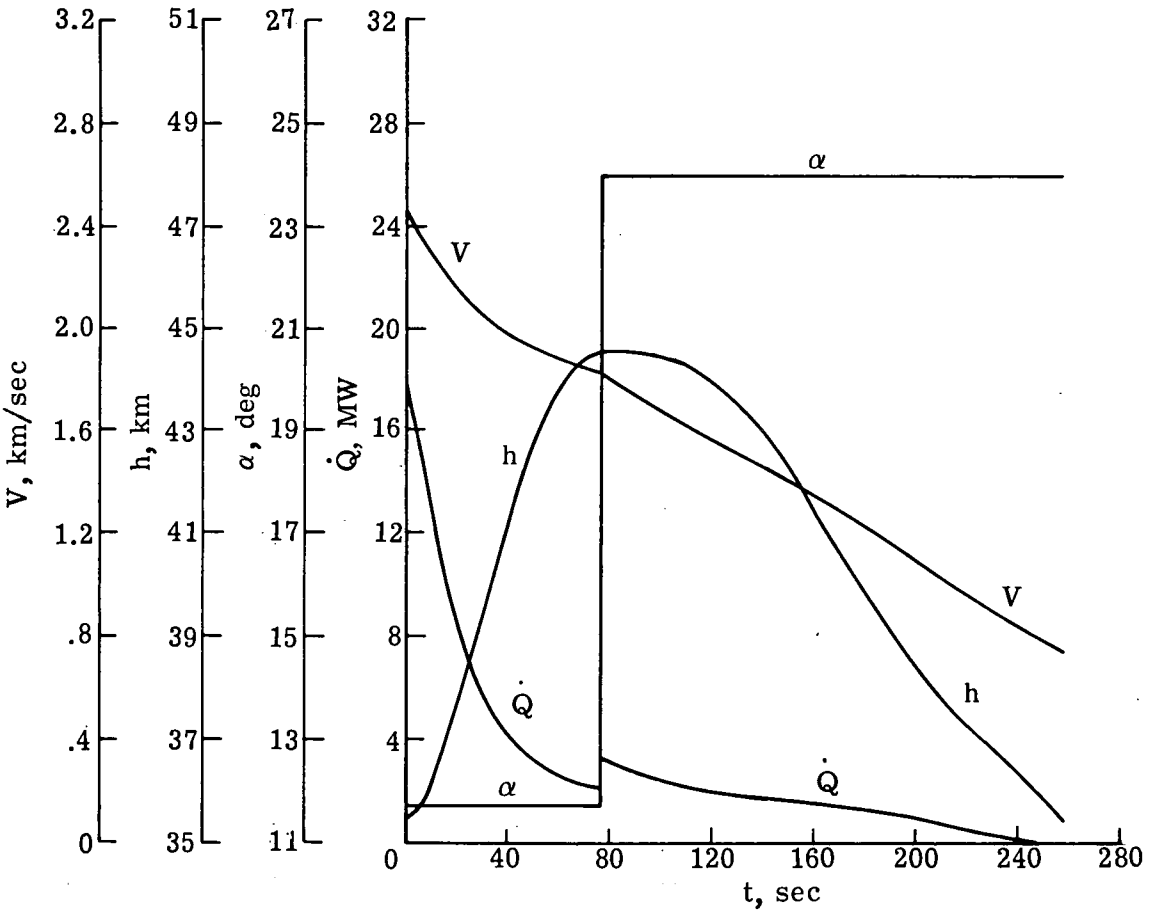

(b) $S/S_R = 0.16$.

Figure 18.- Concluded.

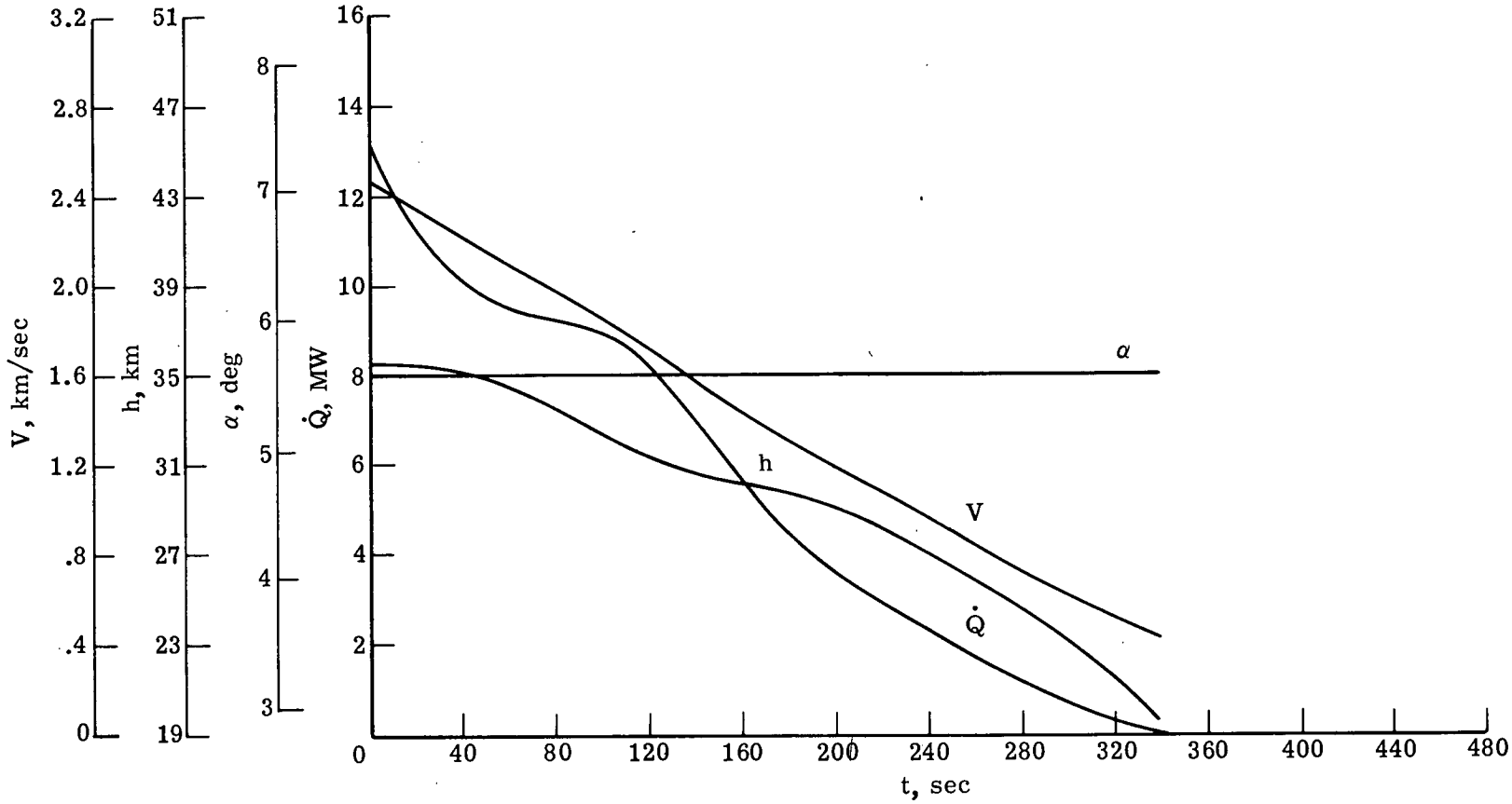

(a) $S/S_R = 0.08$.

Figure 19.- Drag brakes added to nominal descent (descent at cruise angle of attack).

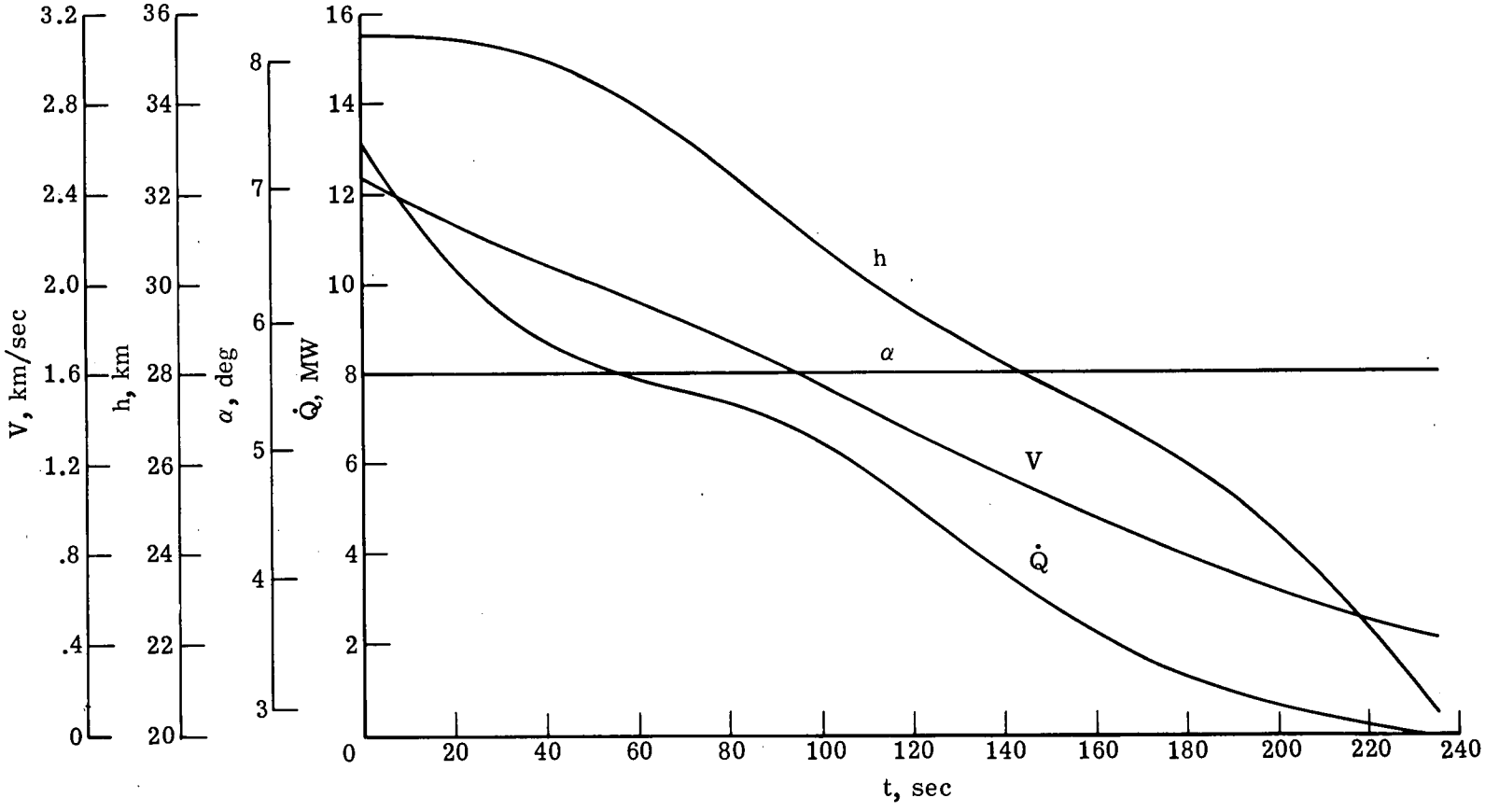

(b) $S/S_R = 0.16$.

Figure 19.- Concluded.

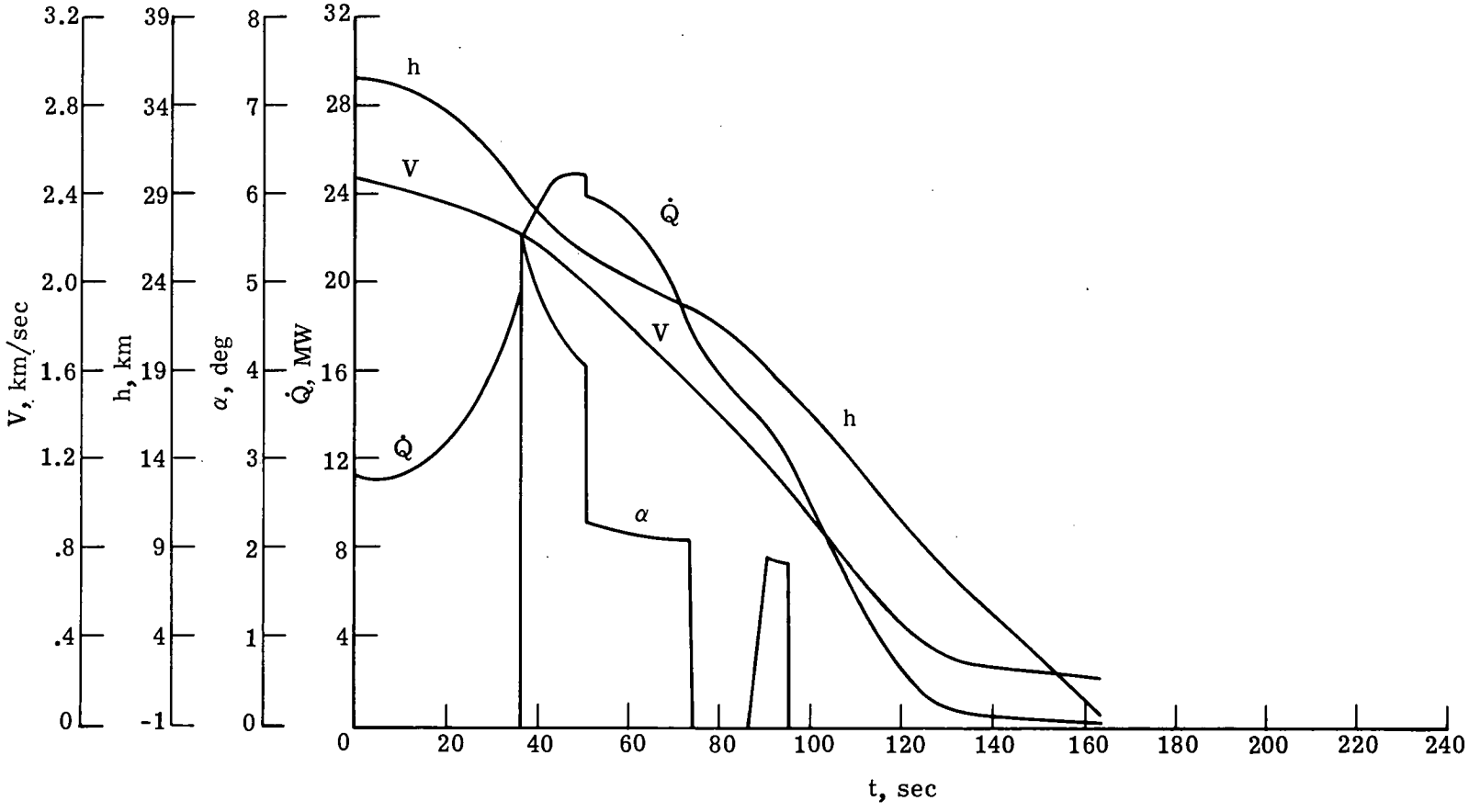

(a) $S/S_R = 0.08$.

Figure 20.- Drag brakes added to high-dynamic-pressure descent.

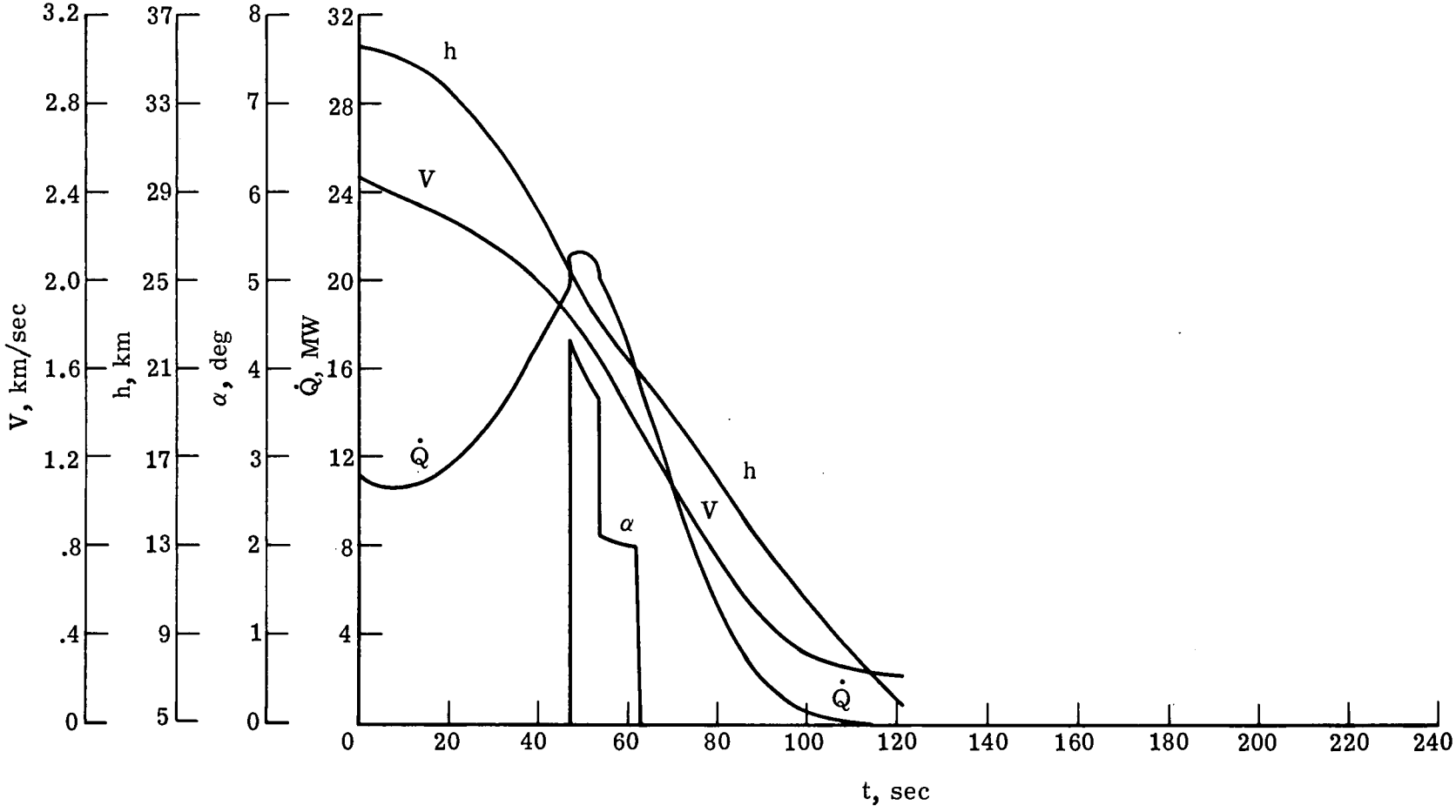

(b) $S/S_R = 0.16$.

Figure 20.- Concluded.

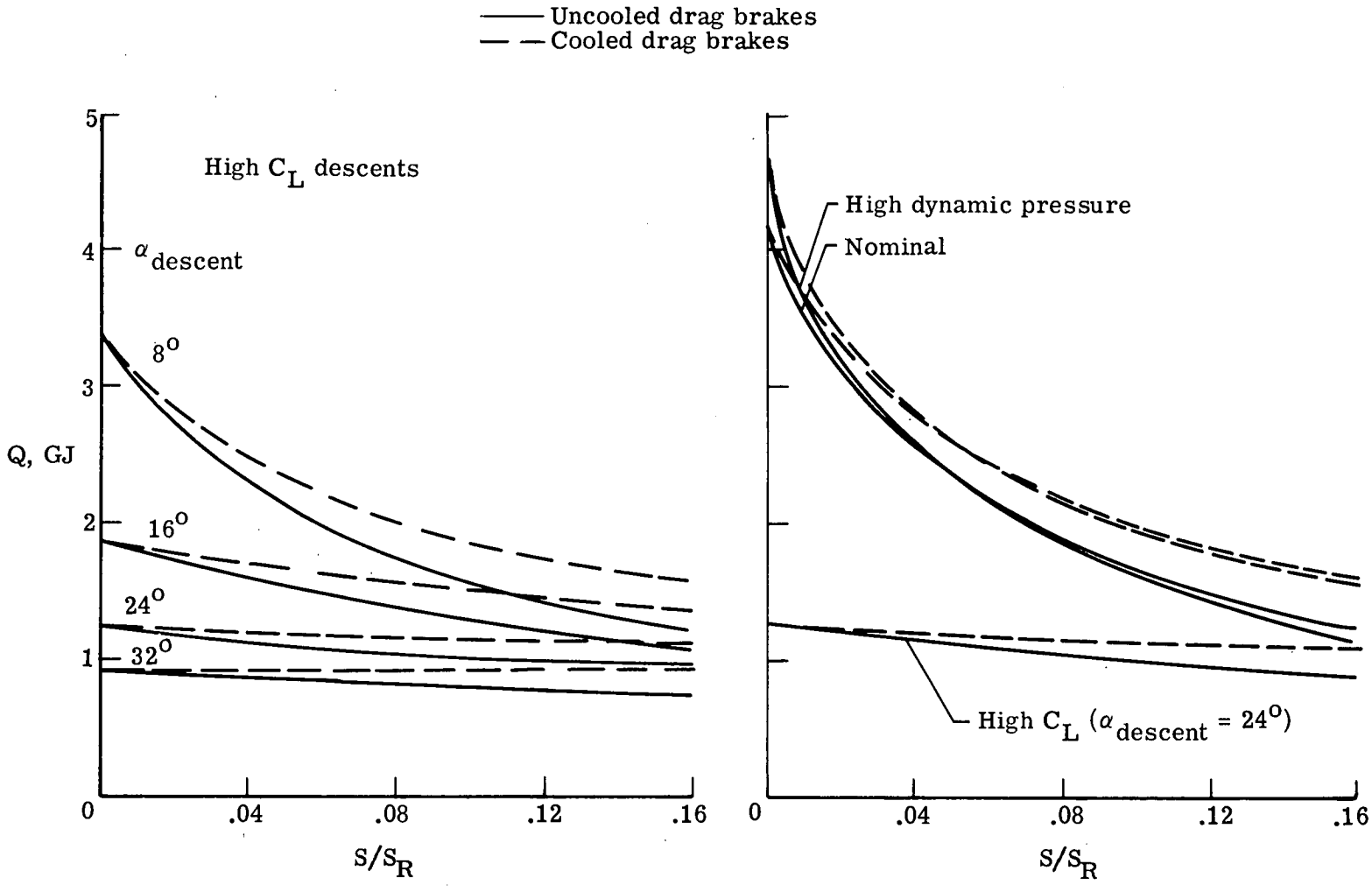

Figure 21.- Variation in aircraft total heat load with drag-brake size for cooled and uncooled drag brakes for several descent types. M = 8; q = 23.94 kPa (500 lb/ft^2).

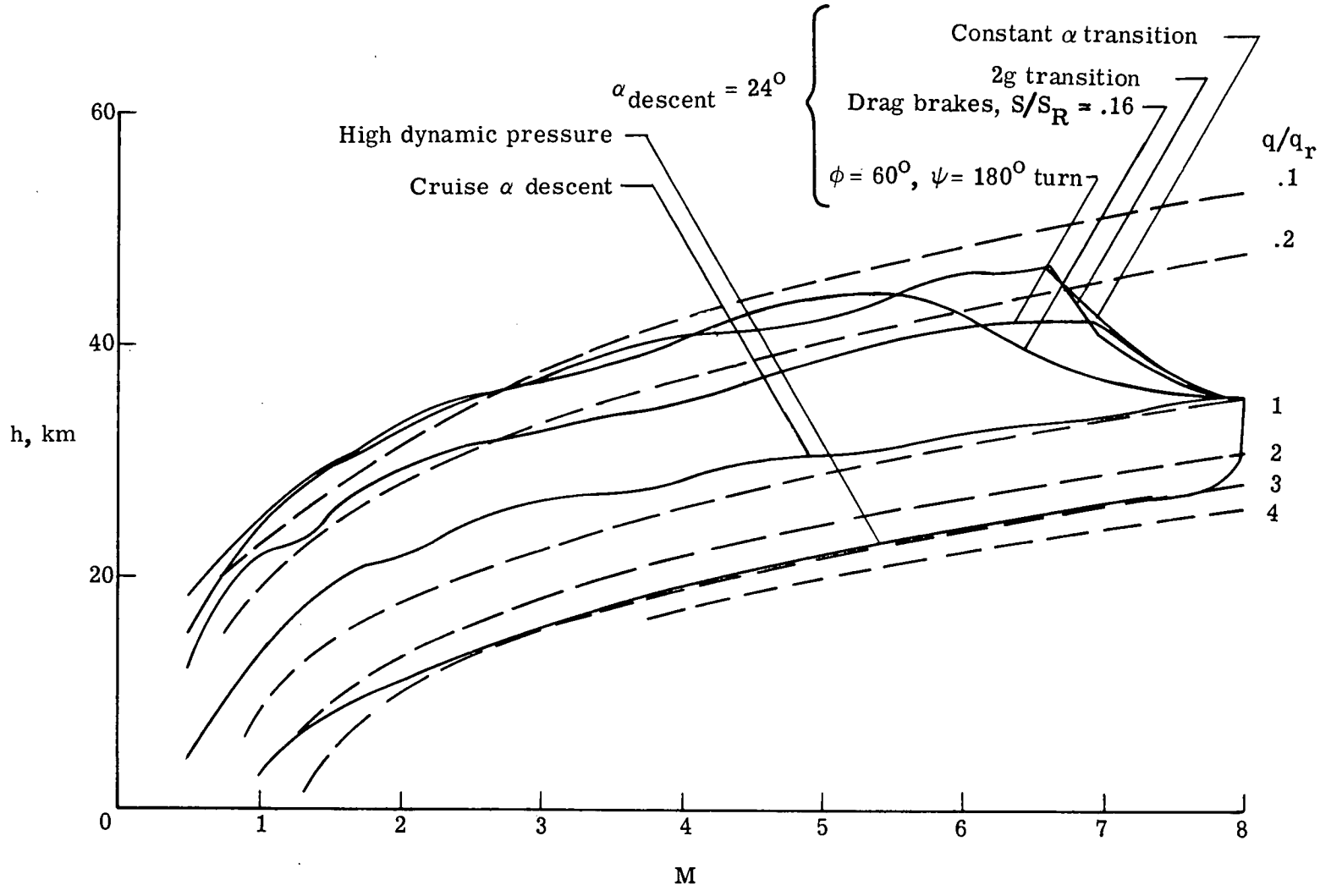

Figure 22.- Comparison of various descents from reference cruise condition: $M_c = 8$; $q_r = 23.94$ kPa (500 lb/ft^2).

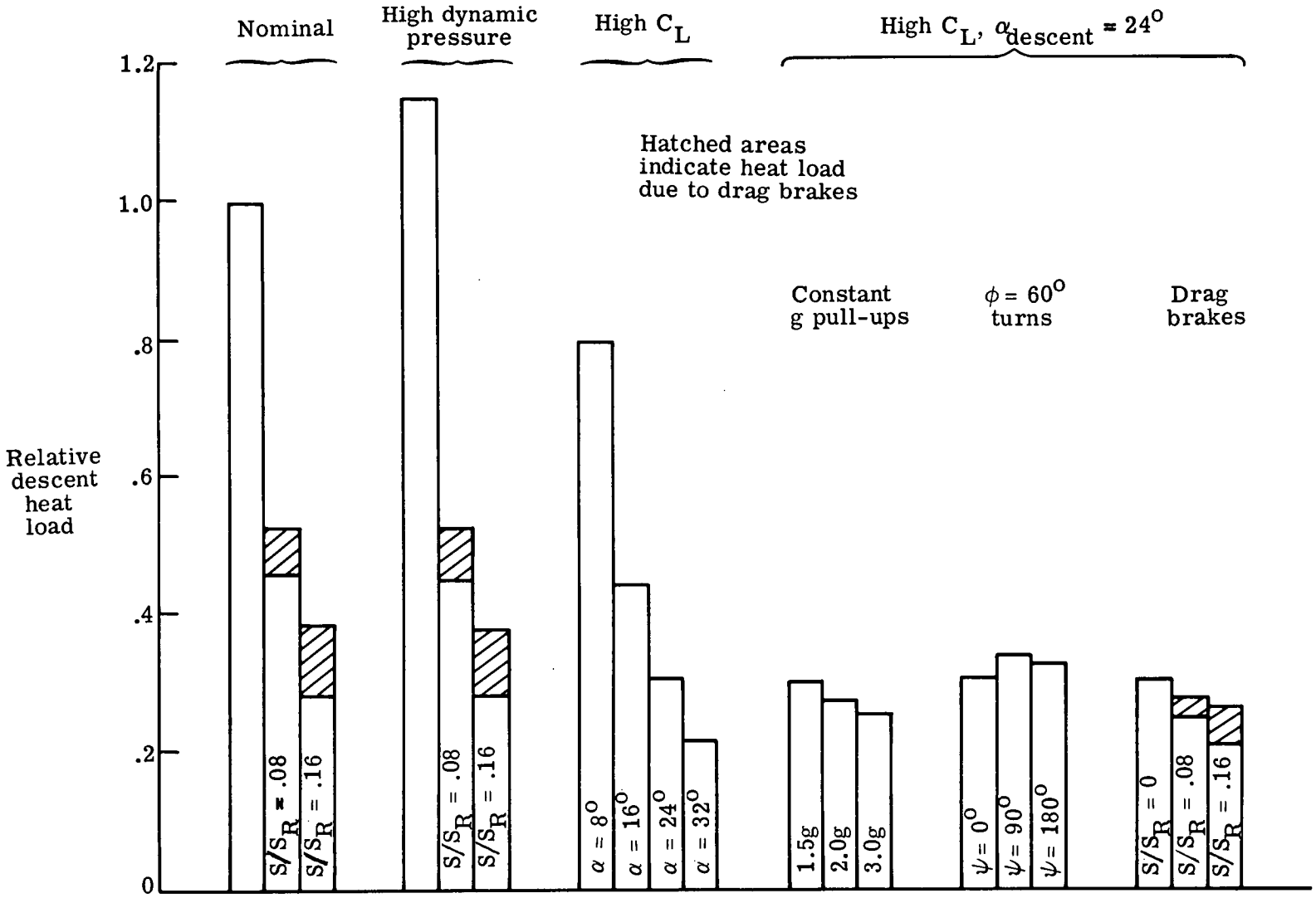

Figure 23.- Comparison of total heat loads for each descent type. $M_c = 8$; $q_r = 23.94$ kPa (500 lb/ft^2).

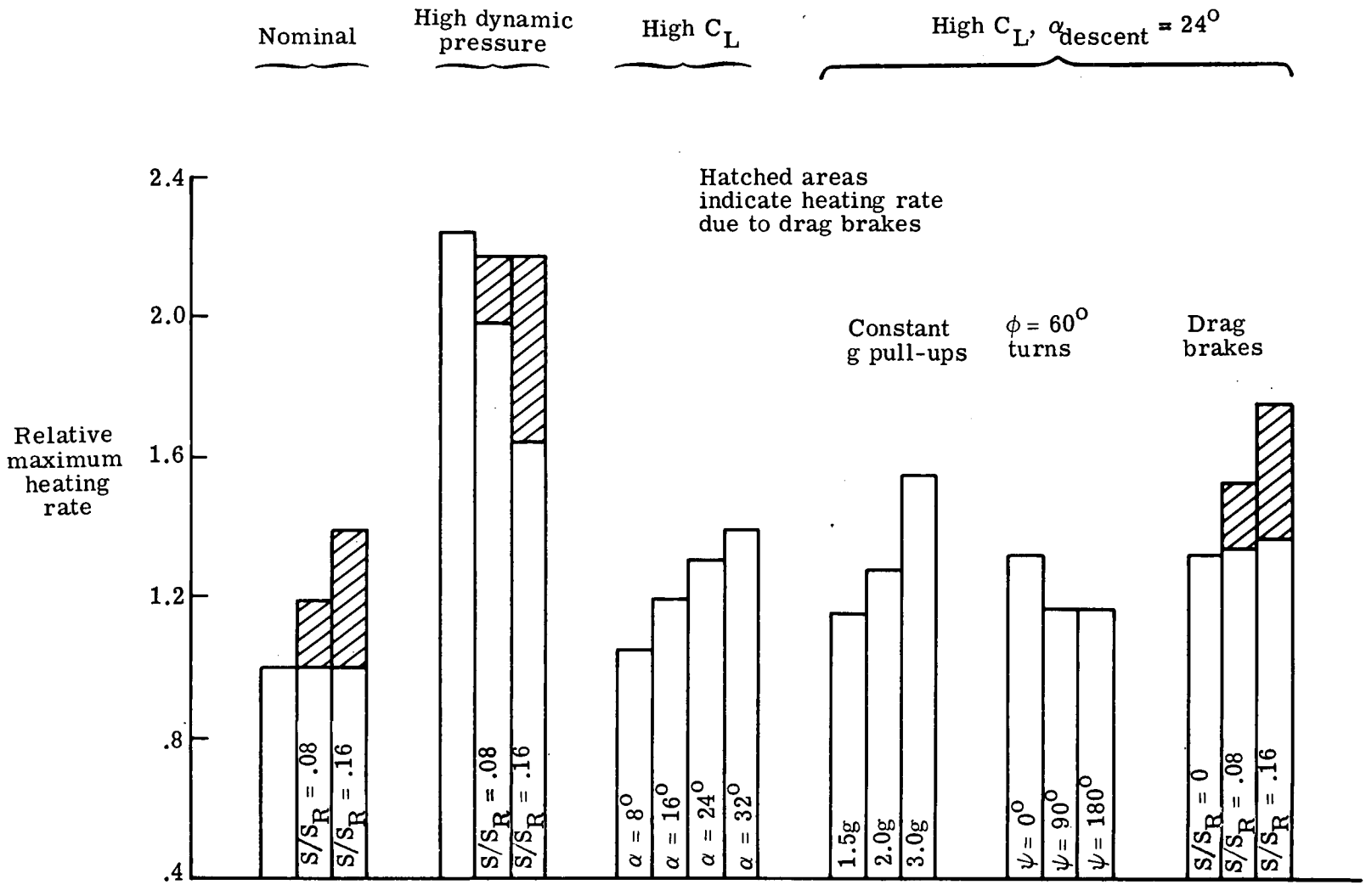

Figure 24.- Comparison of peak heating rates for each descent type.

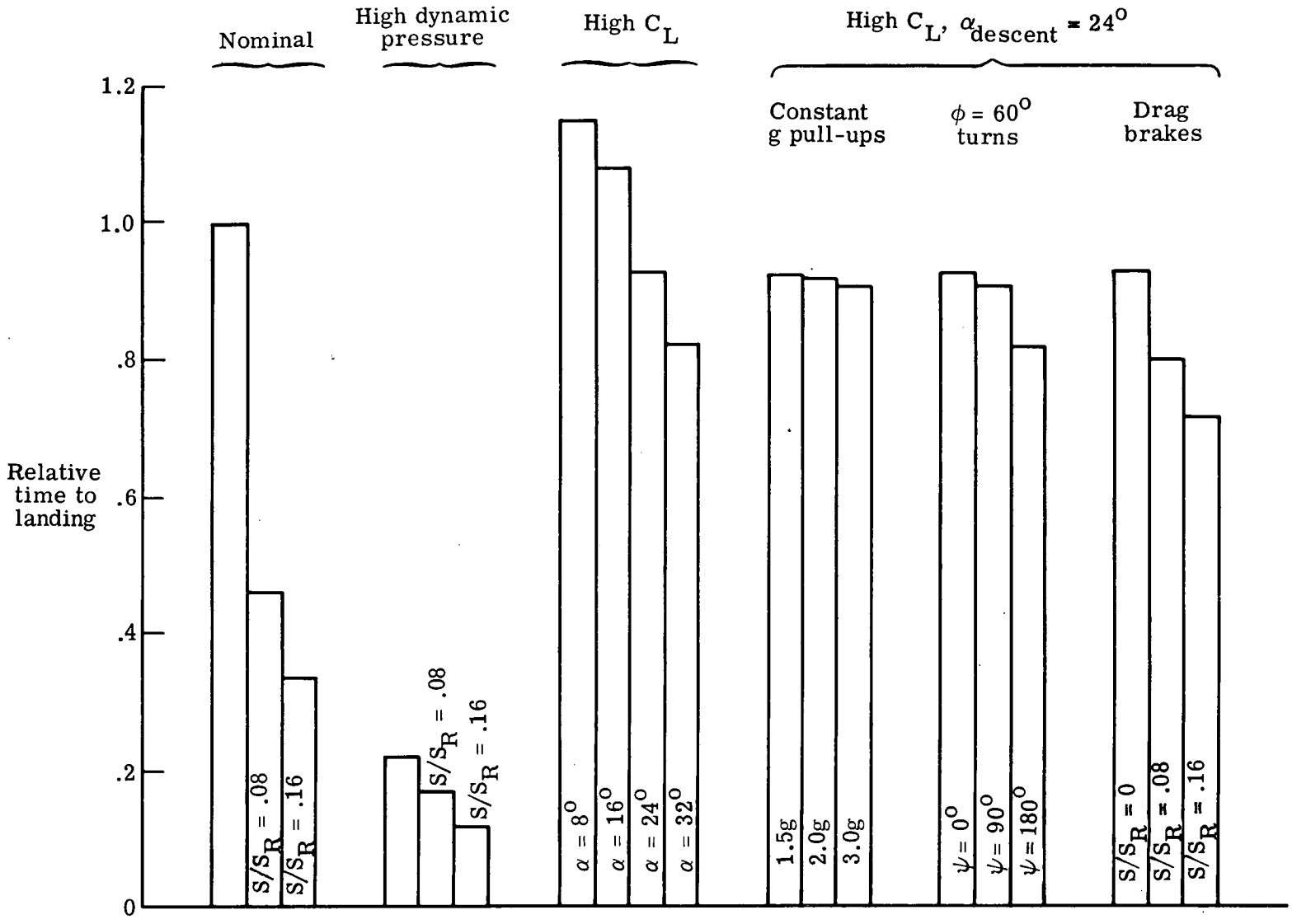

Figure 25.- Comparison of time from cruise to landing for each descent type.

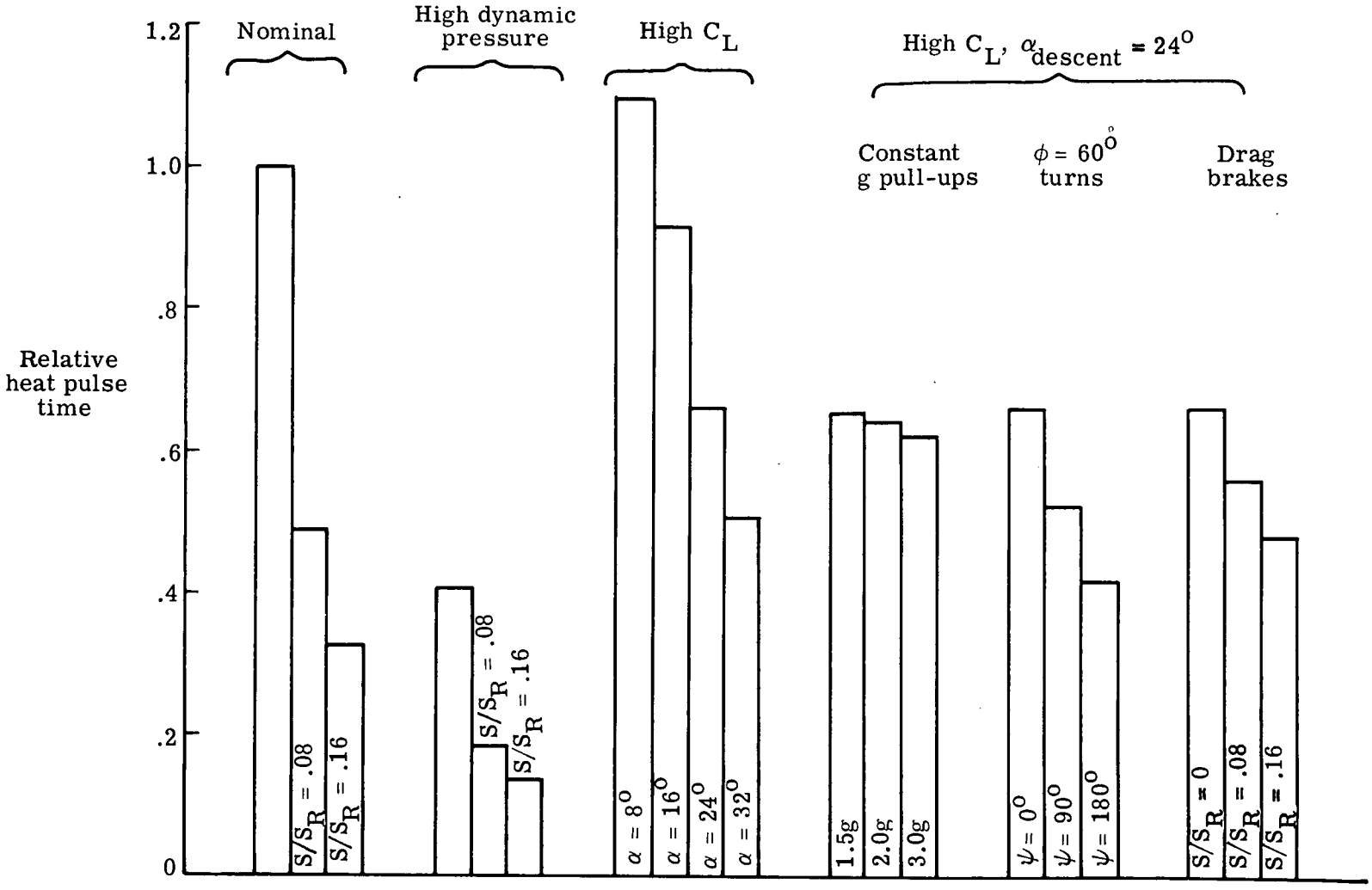

Figure 26.- Comparison of time to end of heat pulse for each descent type.

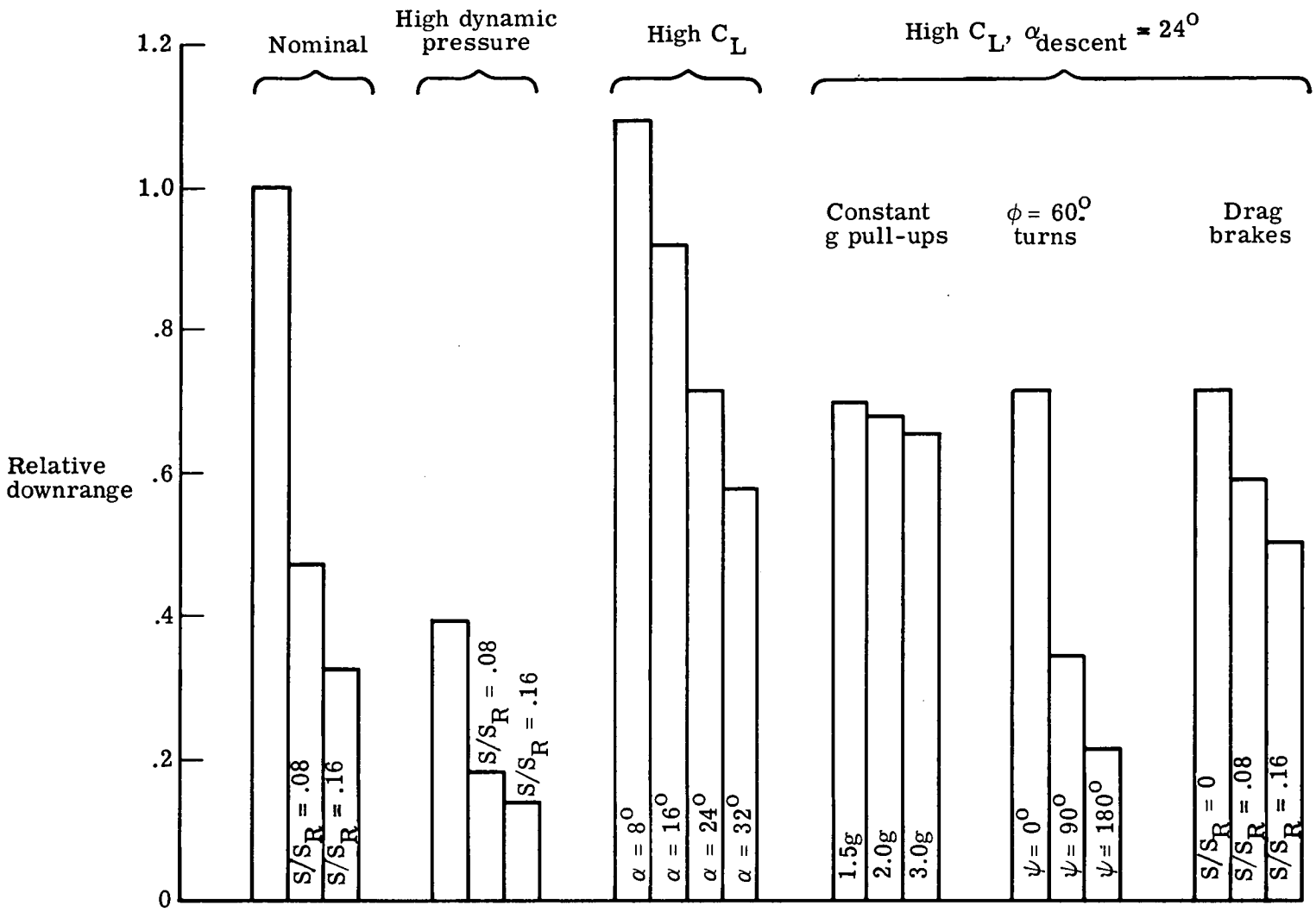

Figure 27.- Comparison of downrange for each descent type.

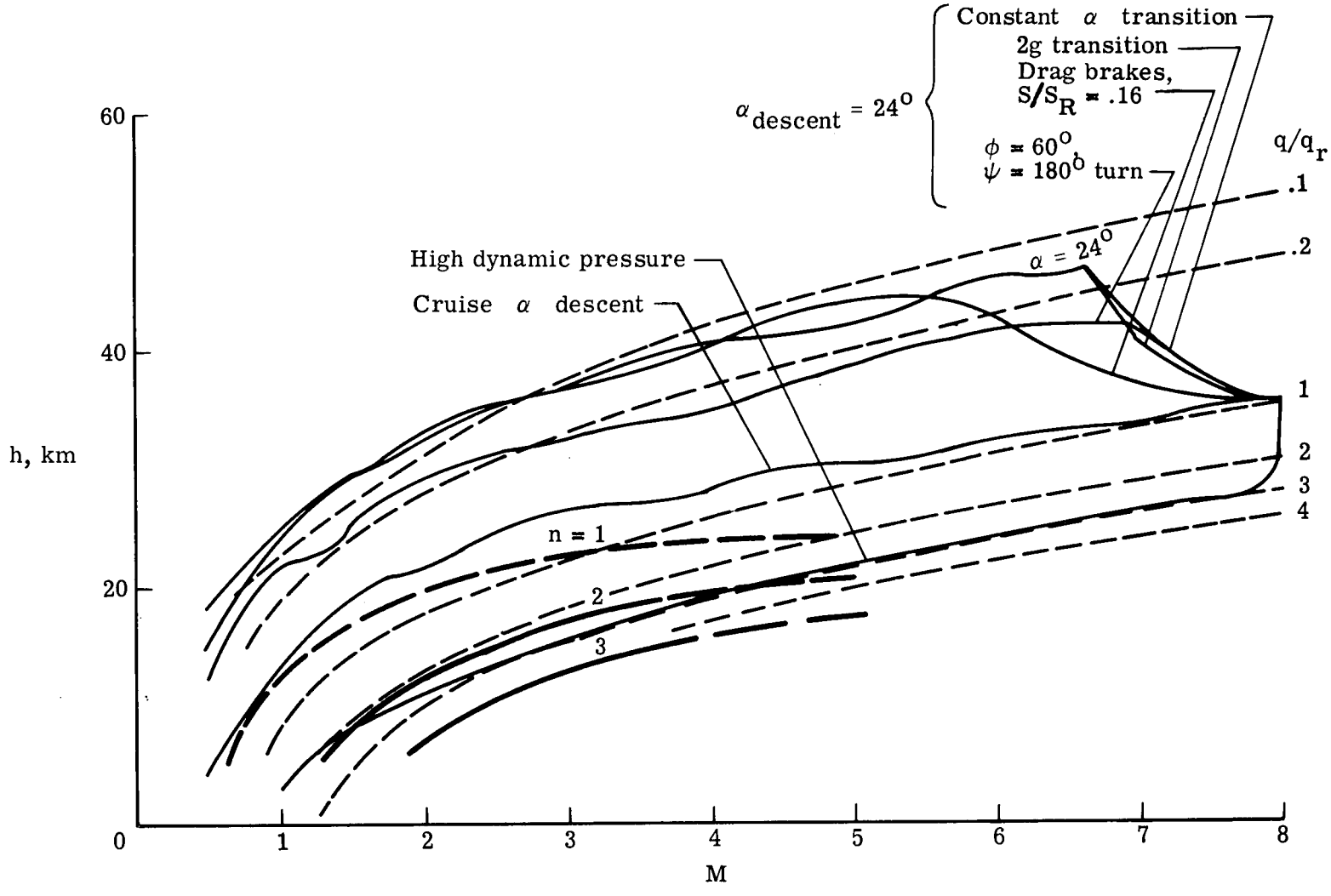

Figure 28.- Additive loads due to gusts.

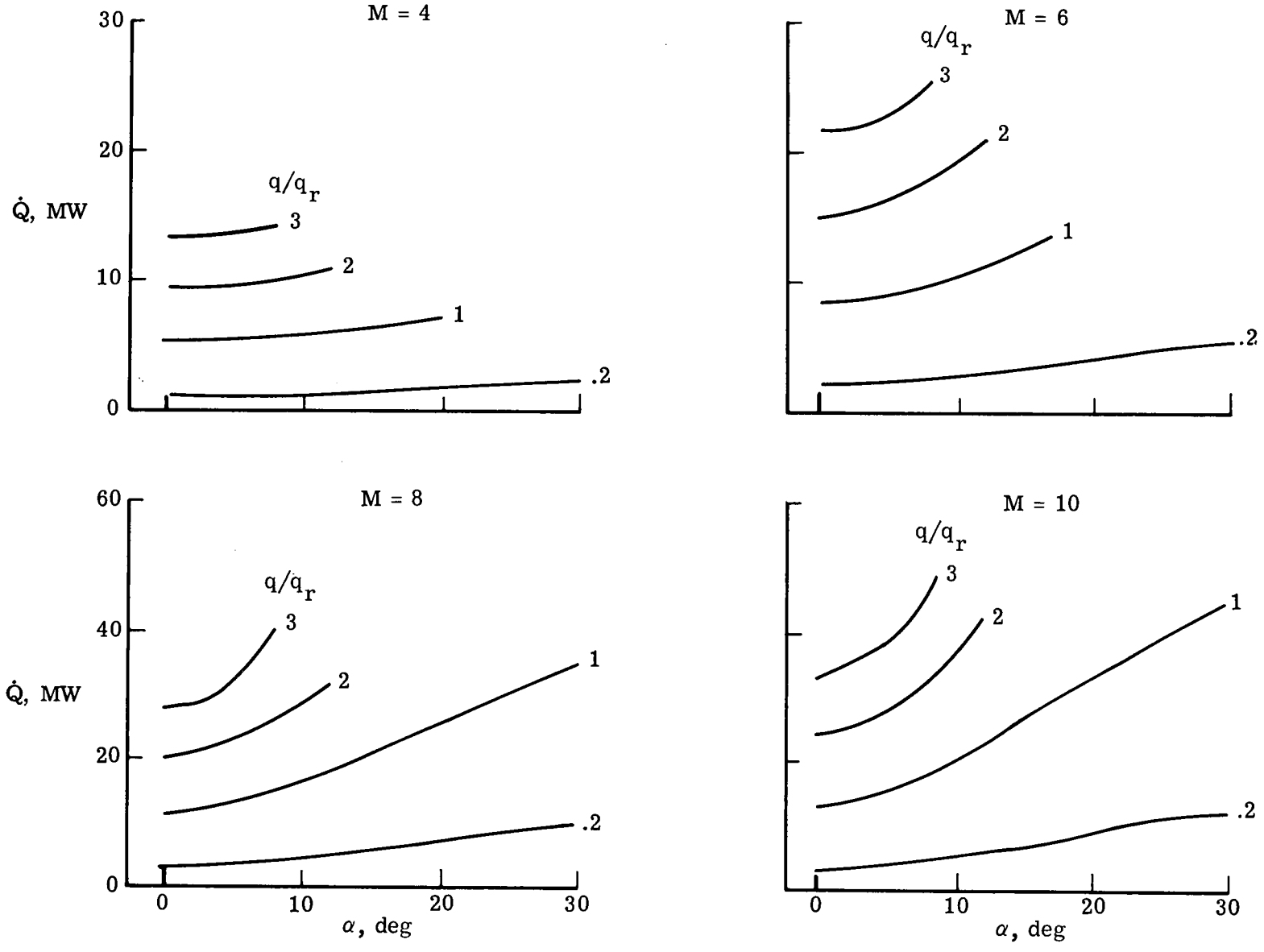

Figure 29.- Aircraft heating rates as a function of angle of attack for several Mach numbers and dynamic-pressure ratios.

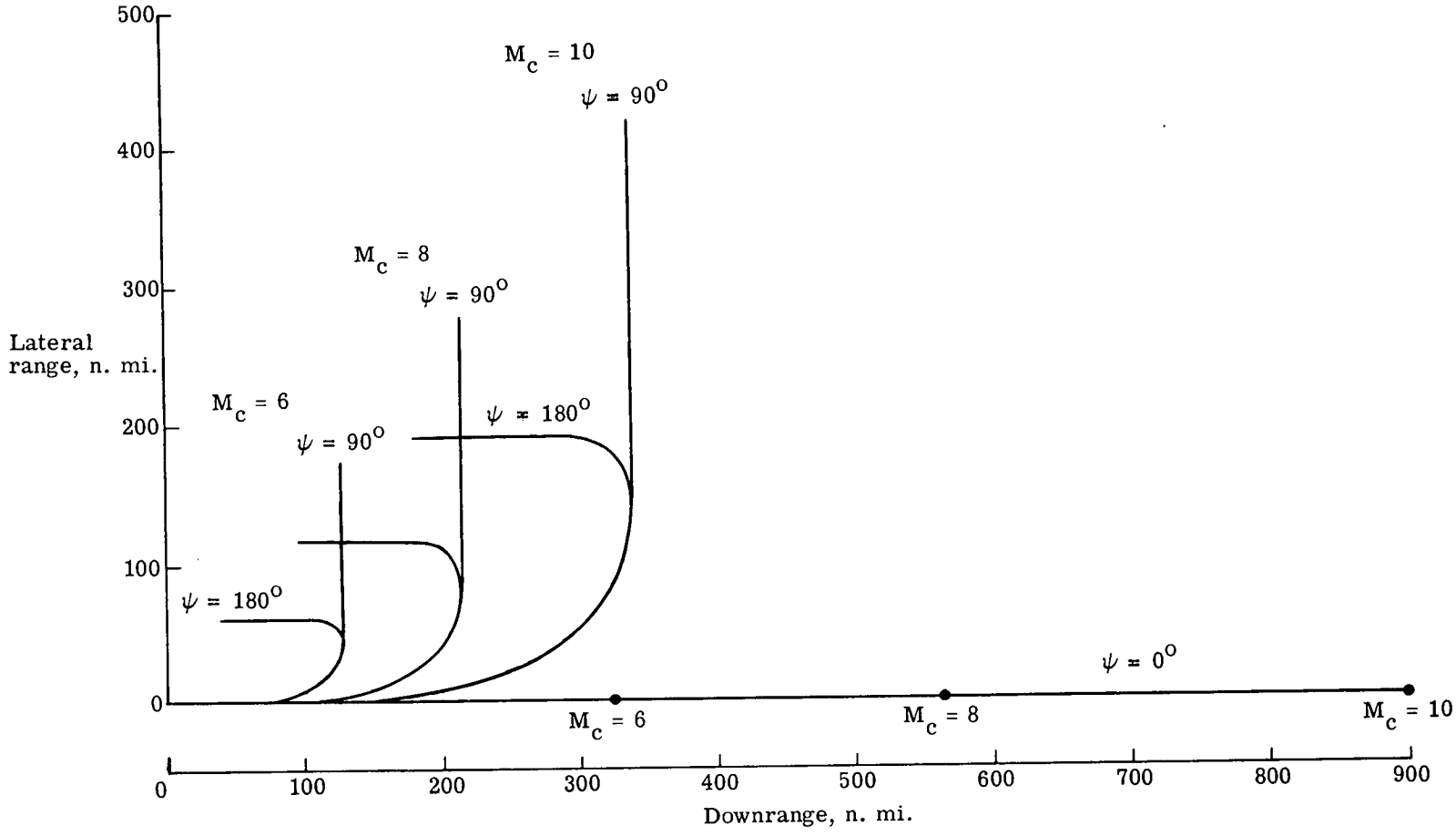

(a) $\alpha_{descent} = 16^{o}$.

Figure 30.- Lateral range and downrange for turning descents for final heading angles of 0^{o}, 90^{o}, and 180^{o} and cruise Mach numbers of 6, 8, and 10. q = 23.94 kPa (500 lb/ft^2).

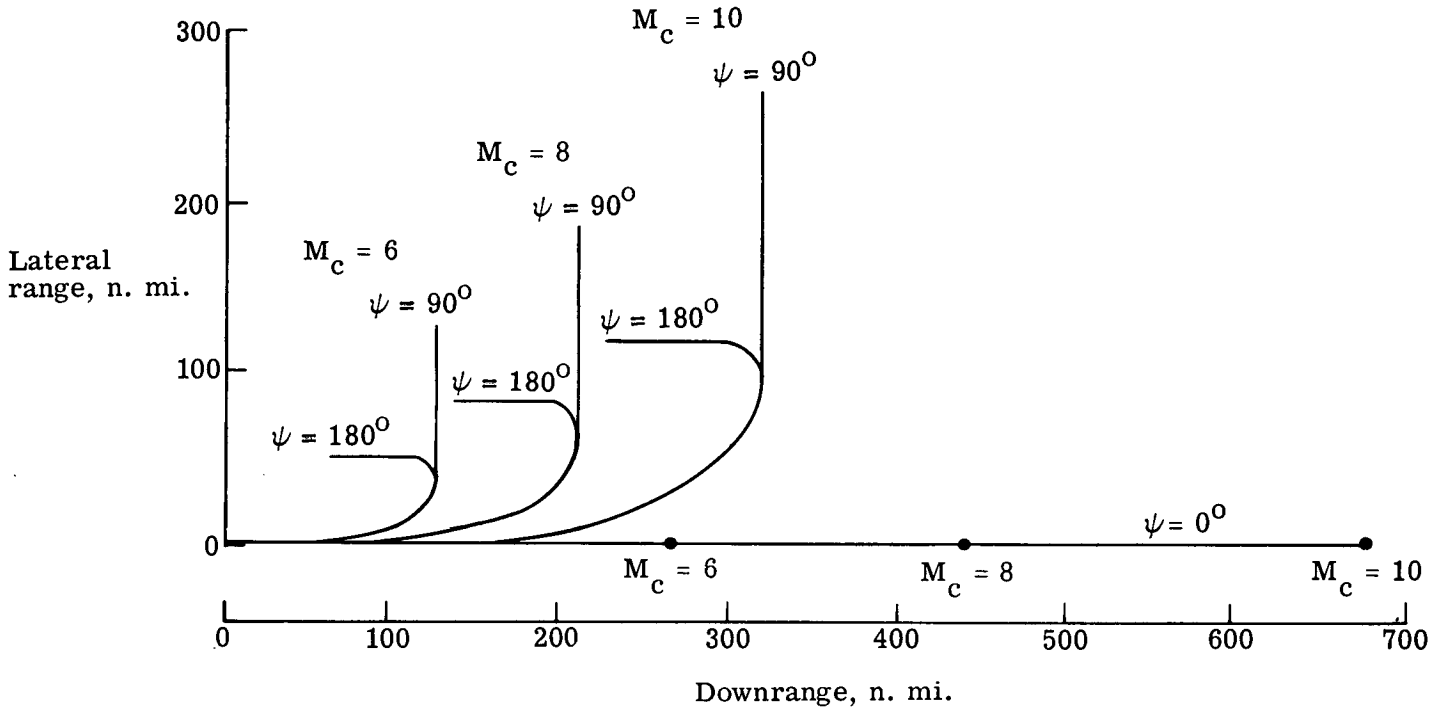

(b) $\alpha_{descent} = 24^{\circ}$.

Figure 30.- Continued.

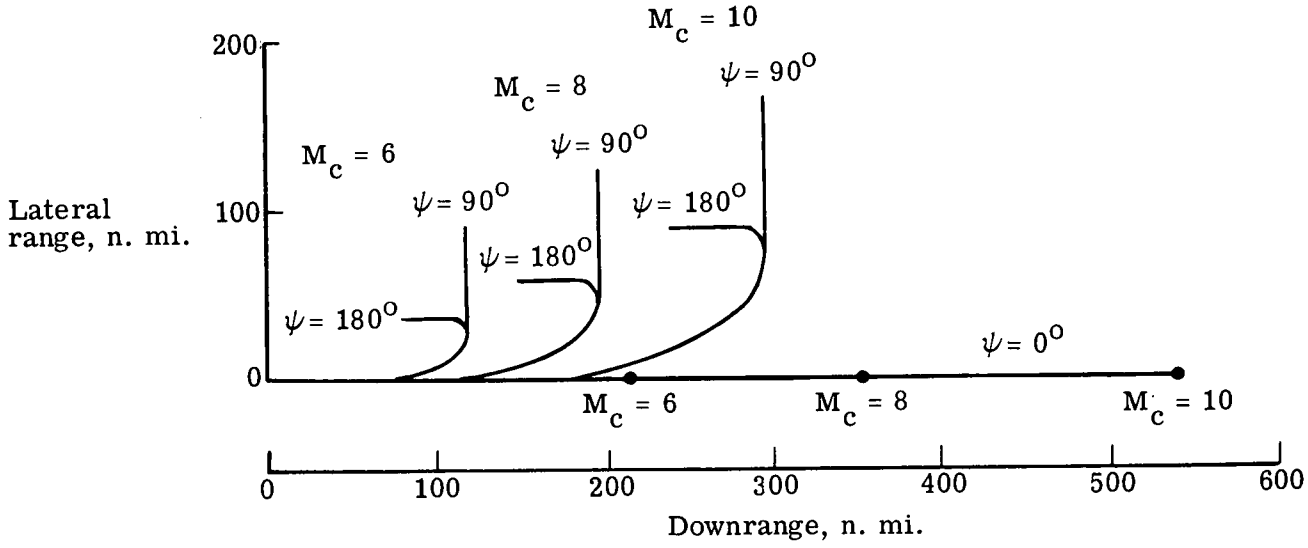

(c) $\alpha_{descent} = 32^{o}$.

Figure 30.- Concluded.

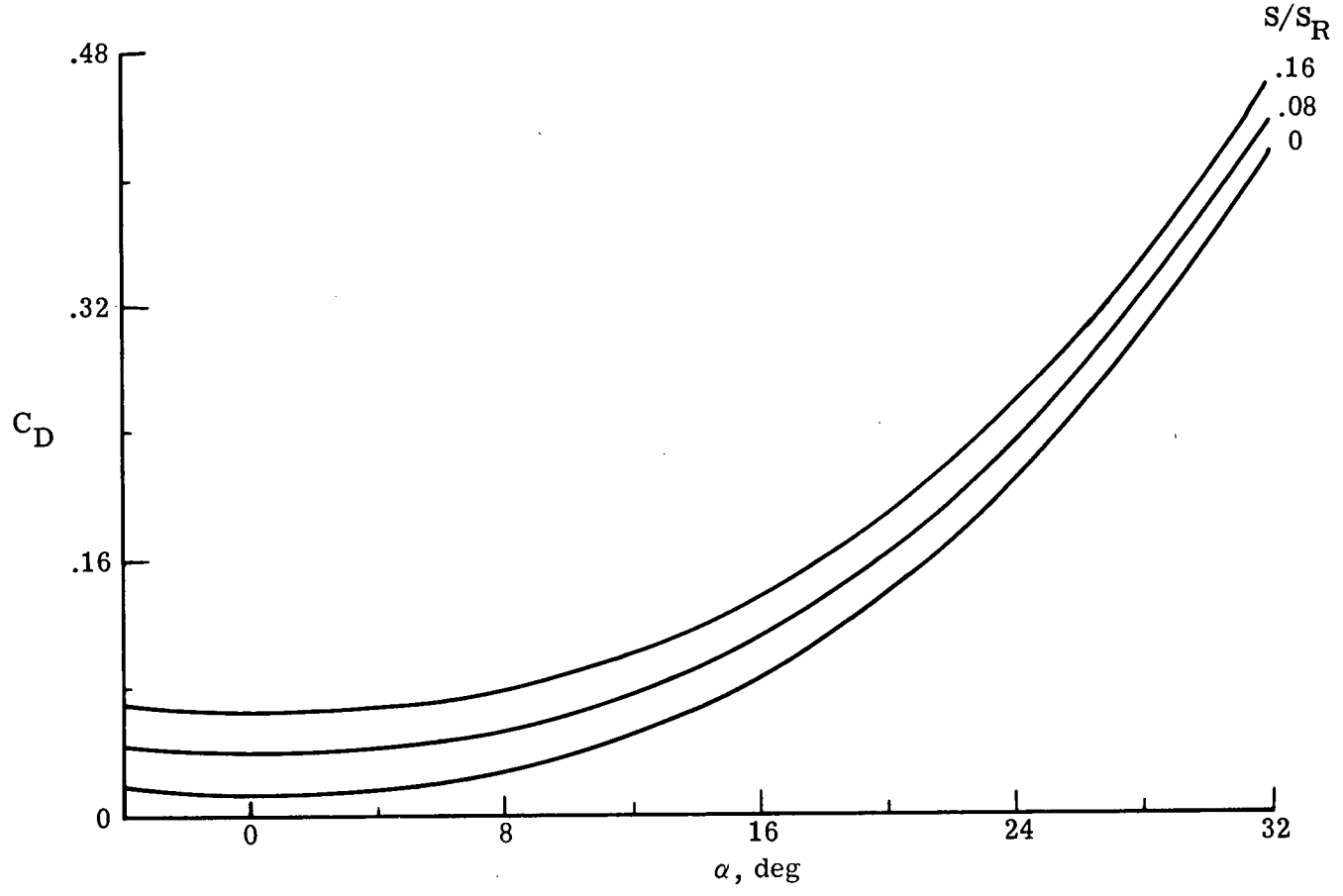

Figure 31.- Variation of drag coefficient with angle of attack and drag-brake size. M = 8; q = 23.94 kPa (500 lb/ft^2).

NATIONAL AERONAUTICS AND SPACE ADMINISTRATION
WASHINGTON, D.C. 20546

OFFICIAL BUSINESS
PENALTY FOR PRIVATE USE $300

SPECIAL FOURTH-CLASS RATE
BOOK

POSTAGE AND FEES PAID
NATIONAL AERONAUTICS AND
SPACE ADMINISTRATION
451

U.S.MAIL

POSTMASTER : If Undeliverable (Section 158 Postal Manual) Do Not Return

"The aeronautical and space activities of the United States shall be conducted so as to contribute . . . to the expansion of human knowledge of phenomena in the atmosphere and space. The Administration shall provide for the widest practicable and appropriate dissemination of information concerning its activities and the results thereof."

—NATIONAL AERONAUTICS AND SPACE ACT OF 1958

NASA SCIENTIFIC AND TECHNICAL PUBLICATIONS

TECHNICAL REPORTS: Scientific and technical information considered important, complete, and a lasting contribution to existing knowledge.

TECHNICAL NOTES: Information less broad in scope but nevertheless of importance as a contribution to existing knowledge.

TECHNICAL MEMORANDUMS: Information receiving limited distribution because of preliminary data, security classification, or other reasons. Also includes conference proceedings with either limited or unlimited distribution.

CONTRACTOR REPORTS: Scientific and technical information generated under a NASA contract or grant and considered an important contribution to existing knowledge.

TECHNICAL TRANSLATIONS: Information published in a foreign language considered to merit NASA distribution in English.

SPECIAL PUBLICATIONS: Information derived from or of value to NASA activities. Publications include final reports of major projects, monographs, data compilations, handbooks, sourcebooks, and special bibliographies.

TECHNOLOGY UTILIZATION PUBLICATIONS: Information on technology used by NASA that may be of particular interest in commercial and other non-aerospace applications. Publications include Tech Briefs, Technology Utilization Reports and Technology Surveys.

Details on the availability of these publications may be obtained from:

SCIENTIFIC AND TECHNICAL INFORMATION OFFICE

NATIONAL AERONAUTICS AND SPACE ADMINISTRATION

Washington, D.C. 20546